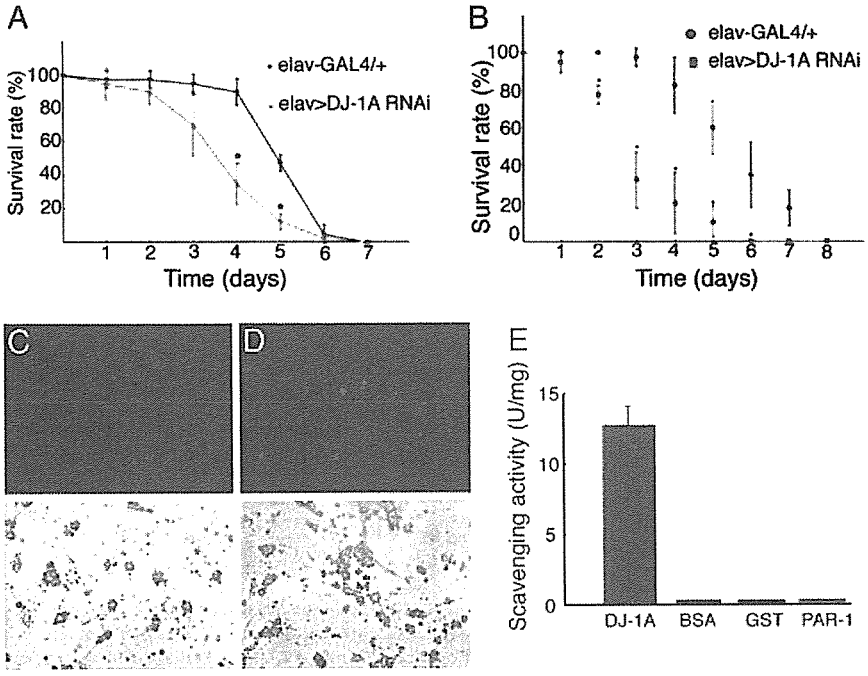

Fig. 3. DJ-1A RNAi leads to ROS accumulation and hypersensitivity to oxidative stress. (*A* and *B*) Comparison of survival curves of *elav-GAL4* flies with *elav-GAL4 DJ-1A RNAi* flies that are treated with 1% H2O2 (*A*) or 100 mM 3-AT (*B*). (*C* and *D*) DCFH-DA staining of cultured *Da-GAL4* (*C*) and *Da-GAL4 DJ-1A RNAi* (*D*) neurons. (*Upper*) Fluorescent DCFH-DA staining in green. (*Lower*) Black and white images of the neuronal culture being analyzed. (*E*) Recombinant DJ-1A protein exhibits detectable *in vitro* H_2O_2 scavenging activity, whereas the control proteins BSA, GST, and PAR-1 have no such activity.

which only showed weak ROS staining in a small percentage of neurons, *DJ-1A RNAi* neuronal culture had more neurons stained by this dye, and the staining intensity was much higher (Fig. 3, compare *D* with *C*).

Human DJ-1 protein was previously shown to be able to eliminate H2O2 *in vitro* by oxidizing itself at specific Cys residues (10, 27). To test whether *Drosophila* DJ-1A has similar H_2O_2 scavenging activity, we incubated bacterially expressed recombinant DJ-1A protein with H_2O_2 in test tubes and measured the conversion of H_2O_2. DJ-1A protein was found to have a specific activity in scavenging H_2O_2, whereas a control BSA protein has no such activity (Fig. 3*E*). This activity may not be simply attributed to nonspecific reaction of H_2O_2 with Cys residues, because the amino acid composition of BSA has a higher percentage of Cys residues than DJ-1A. Instead, this result indicates that DJ-1A may possess a specific activity in eliminating H_2O_2. In addition to BSA, which is normally resides in an extracellular environment, two intracellular proteins, GST and the Ser Thr protein kinase PAR-1, also showed no H_2O_2 scavenging activity. It should be noted that the H_2O_2 scavenging activity of DJ-1A was two orders of magnitude lower than that of catalase in the same assay (20 units mg vs. 2,300 units mg), suggesting that degrading H_2O_2 may not be the main function of DJ-1A.

Modulation of DJ-1A RNAi-Induced Cell Death by the PI3K Akt-Signaling Pathway. In an effort to understand how DJ-1A dysfunction leads to neuronal death, we tested possible genetic modification of DJ-1A RNAi-induced eye phenotypes by candidate genes and signaling pathways previously implicated in cell survival regulation. To see the genetic interaction more clearly, we used the weak RNAi phenotype induced by one copy each of the *GMR-GAL4* and *DJ-1A RNAi* transgenes to score for enhancement; the stronger RNAi phenotype induced by two copies of the *GMR-GAL4* and *DJ-1A RNAi* transgenes was used to score for suppression whenever possible.

The EGF receptor (EGFR) Ras1 mitogen-activated protein kinase (MAPK) signaling pathway has previously been shown to directly target the *Drosophila* proapoptotic gene *head involution defective* (*hid*) in the eye through MAPK-mediated phosphorylation and inactivation of HID (28). By using loss-of-function and gain-of-function alleles of *rolled* (*MAPK*) and loss-of-function alleles of *hid*, we did not detect clear genetic interaction with DJ-1A RNAi flies (data not shown). Similarly, we could not detect clear genetic interaction between DJ-1A RNAi and loss-of-function or overexpression alleles of genes in the JNK pathway, which has also been shown to induced cell death in the eye when activated (29).

In contrast, a clear genetic interaction was detected between DJ-1A and the *Drosophila* PI3K Akt pathway genes. A dramatic enhancement of DJ-1A RNAi-induced eye degeneration was observed when *PTEN* was coexpressed with the DJ-1A RNAi transgene (Fig. 4*D*). The resulting fly eyes were dramatically reduced in size, with collapsed and fused ommatidia and necrotic spots, which were not present in DJ-1A RNAi only flies. Staining of photoreceptor neurons revealed a near complete loss of photoreceptor neurons in *PTEN* coexpression fly eyes (data not shown). Overexpression of this *UAS-PTEN* transgene alone with *GMR-GAL4* driver had little effect on the regular organization of the ommatidia and photoreceptor number per ommatidium, although the overall size of the eye was moderately reduced (Fig. 4*L*). When we tested with a mutant form of human PTEN that contains an inactivating C124S mutation (18), no effect on DJ-1A RNAi phenotype was observed (data not shown). Similar to the effect of *Drosophila PTEN*, an enhancement of the DJ-1A RNAi phenotype was observed when a dominant-negative (DN) form of PI3K catalytic subunit *Dp110* (*PI3K DN*) was coexpressed (17) (Fig. 4*C*), although expression of this *PI3K DN* transgene alone had little effect on eye morphology (Fig. 4*K*).

A clear suppression of DJ-1A RNAi phenotype was observed when the wild-type form of PI3K catalytic subunit *Dp110* was coexpressed. The eyes were restored to normal size, and the organization of the ommatidia was significantly improved (Fig. 4*B*). Overexpression of a *UAS-Akt* transgene had similar effect as *PI3K* in suppressing DJ-1A RNAi-induced toxicity in the eye (Fig. 4*A*), consistent with Akt PKB being a key downstream effecter component in the PI3K-signaling pathway (16).

Given the known pleiotropic function of the PI3K-signaling pathway in regulating cell size and cell number in *Drosophila* and its potential role in regulating cell survival, we next tested the effect of manipulating PI3K pathway gene activity on an eye degeneration phenotype caused by a different mechanism. Overexpression of human *tau* in the fly eye also led to a reduction in eye size and loss of photoreceptor neurons (19, 22). In contrast to the *DJ-1A RNAi*

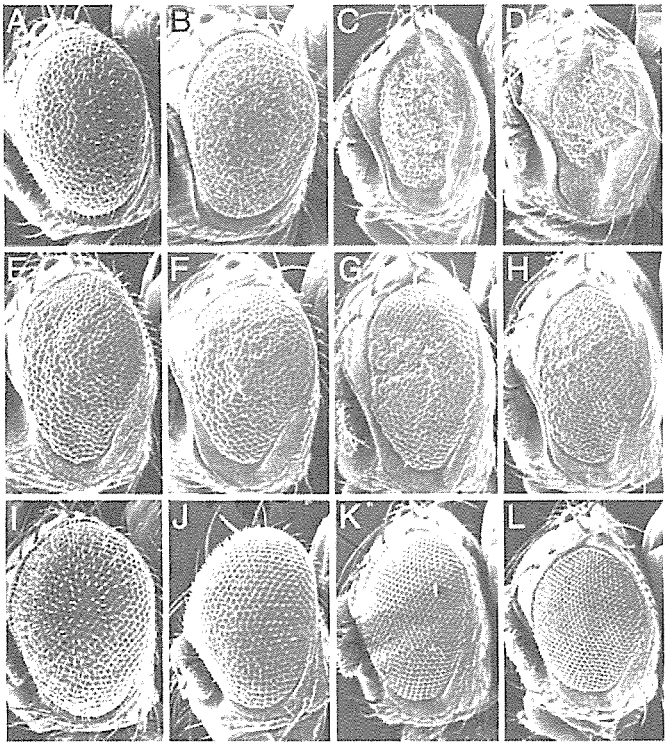

Fig. 4. Modification of DJ-1A RNAi phenotypes by altered expression of genes in the PI3K Akt pathway. (*A–D*) SEM eye images of DJ-1A RNAi flies coexpressing *UAS-Akt* (*A*), *UAS-PI3K Dp110* (*B*), *UAS-PI3K Dp110DN* (*C*), or *UAS-PTEN* (*D*). (*E–H*) SEM eye images of human tauV337M transgenic flies coexpressing *UAS-GFP* (*E*), *UAS-PI3K Dp110* (*F*), *UAS-PI3K Dp110DN* (*G*), or *UAS-PTEN* (*H*). (*I–L*) SEM eye images of flies expressing *UAS-Akt* (*I*), *UAS-PI3K Dp110* (*J*), *UAS-PI3K Dp110DN* (*K*), or *UAS-PTEN* (*L*) transgenes alone. *GMR-GAL4* was used to direct *UAS* transgene expression in all panels.

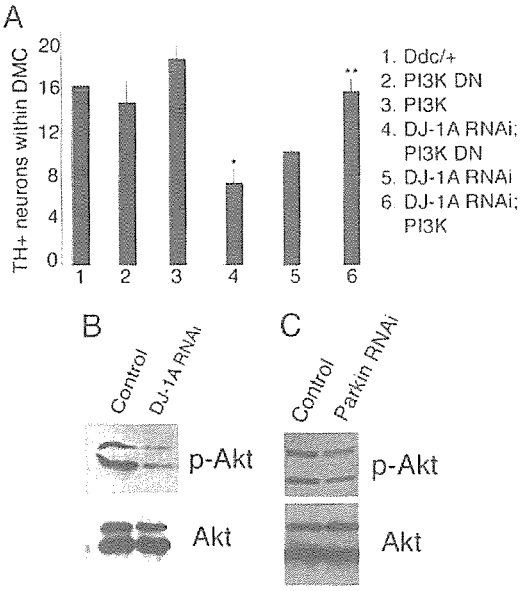

Fig. 5. Modification of DJ-1A RNAi-induced dopaminergic phenotype by altered expression of *PI3K Akt* pathway genes and Western blot analysis showing reduced Akt phosphorylation after DJ-1A or Parkin down-regulation. (*A*) Quantification of TH DA neurons in the DMC of *Ddc-GAL4* control flies, *DJ-1A RNAi* flies, *PI3K* or *PI3K DN* single overexpression flies, and *DJ-1A RNAi* flies coexpressing *PI3K* or *PI3K DN* transgenes. *, P 0.01 in Student's t test. *Ddc-GAL4* was used to direct transgene expression. (*B* and *C*) Western blot analysis of fly head extracts prepared from *Da-GAL4* and *Da-GAL4 DJ-1A RNAi* (*B*) or *Da-GAL4* and *Da-GAL4 dParkin RNAi* (*C*) genotyped flies. Blots were probed with anti-phospho-Akt and anti-Akt antibodies, respectively.

situation, coexpression of wild-type *PI3K*, *PI3K DN*, or *PTEN* showed little effect on human tau-induced toxicity in the eye (Fig. 4, compare *F*, *G*, and *H*, respectively, with *E*). The genetic interaction between DJ-1A and PI3K pathway genes in the eye thus seems to be rather specific.

We next tested the effects of modulating PI3K signaling on the dopaminergic degeneration phenotype induced by DJ-1A RNAi. Coexpression of PI3K completely suppressed the reduction of TH DA neuron phenotype induced by DJ-1A RNAi. The number of DA neurons in the DMCs was maintained at the wild-type level in all of the transgenic flies and at all ages examined (Fig. 5*A*), indicating that coexpression of PI3K blocked DJ-1A RNAi-induced age-dependent dopaminergic degeneration. Conversely, coexpression of PI3K DN showed a statistically significant enhancement of DJ-1A RNAi toxicity in dopaminergic neurons (Fig. 5*A*).

We next examined the effect of PI3K signaling on DJ-1A RNAi-induced ROS accumulation. We found that, in adult fly brain, induction of DJ-1A RNAi within dopaminergic neurons led to an elevation of ROS levels, consistent with neuronal culture studies described earlier (Fig. 7*A*, which is published as supporting information on the PNAS web site). Inhibition of PI3K signaling in these neurons by means of overexpression of PI3K DN also led to elevation of ROS levels (Fig. 7*B*), whereas flies overexpressing wild-type PI3K showed basal ROS levels (Fig. 7*C*). Strikingly, in DJ-1A RNAi flies coexpressing PI3K, cellular ROS levels are reduced to baseline levels as in wild-type controls (Fig. 7*G*). Together, these results indicate that PI3K signaling specifically suppresses DJ-1A RNAi-induced neurotoxicity and that this suppression is correlated with a reduction of cellular ROS levels.

DJ-1A RNAi Flies and Parkin Mutant Flies Exhibit Impaired PI3K Akt Signaling. The fact that increased PI3K Akt signaling specifically suppressed DJ-1A RNAi-induced cell death suggests that the cell death in DJ-1A RNAi animals may be caused by a reduction of PI3K Akt signaling. To test this possibility, we examined the phosphorylation status of Akt, an indicator of PI3K Akt signaling, in DJ-1A RNAi animals. Head extracts from *Da-GAL4* and *Da-GAL4 DJ-1A RNAi* animals were analyzed by Western blot analysis by using anti-phospho-Akt and anti-Akt antibodies. As shown in Fig. 5*B*, although the level of total Akt protein was comparable between control and DJ-1A RNAi fly heads, the amount of phospho-Akt was significantly reduced in *DJ-1A RNAi* animals. This result indicates that DJ-1A down-regulation leads to hypophosphorylation of Akt and impairment of PI3K Akt signaling in the fly brain. To test whether impairment of PI3 Akt signaling is a general feature of PD models, we analyzed the *Drosophila parkin* model. As shown in Fig. 5*C*, inhibition of Parkin function also led to a reduction of phospho-Akt levels. These results implicate reduced PI3K Akt signaling as a common molecular event in the pathogenic cascade of PD.

Discussion

Loss-of-function mutations in human DJ-1 are linked to familial Parkinson's disease. The exact molecular function of DJ-1 that is relevant to disease pathogenesis is not well understood. Our results suggest that *Drosophila* DJ-1A plays an important role in cellular ROS homeostasis and protection against oxidative stress. This conclusion is consistent with previous studies in mammalian cell culture and DJ-1 knockout mice (13, 27, 30). Human DJ-1 was found to have H_2O_2-scavenging activity *in vitro*. (10) (27). Our analysis of *Drosophila* DJ-1A protein supported this notion. However, the H_2O_2-converting activity of DJ-1A is rather low compared with catalase, suggesting that the main molecular function of DJ-1 may not be limited to degrading H_2O_2. It is possible that the ability

to react with H_2O_2 by means of oxidation-sensitive Cys residues may allow DJ-1 to act as a "sensor" of cellular ROS levels, and the oxidized DJ-1 may subsequently acquire a new function to defend against ROS-induced cellular damages. This result would be analogous to the switch of two yeast peroxiredoxins from peroxidase to molecular chaperone under oxidative stress (31). The recent description of human DJ-1 gaining molecular chaperone activity *in vitro* under oxidative conditions is consistent with this model (32).

To understand the cellular processes that mediated DJ-1A dysfunction-induced cell death, we performed genetic interaction studies with genes and signaling pathways that are involved in cell survival and identified components of the PI3K PTEN Akt pathway as modulators of DJ-1 RNAi-induced cell death phenotype. Increase of PI3K Akt-signaling capacity showed suppression, whereas decreased PI3K Akt signaling enhanced DJ-1A RNAi phenotypes. The effects of modulating PI3K Akt signaling on DJ-1A RNAi-induced toxicity hold true in both photoreceptor neurons in the retina and dopaminergic neurons in the central brain, suggesting that the connection between DJ-1 and PI3K Akt signaling is a general phenomenon. The finding that DJ-1A RNAi animals showed decreased phosphorylation of Akt indicate that DJ-1 is a regulator of PI3K Akt signaling. A recent study by Kim *et al.* (15) identified DJ-1A as a suppressor of PTEN function in the fly eye, and the authors further extended this finding to mammalian cells and showed that DJ-1 knockdown by small interfering RNA results in decreased phosphorylation of PKB Akt, whereas DJ-1 overexpression leads to PKB Akt hyperphosphorylation and increased cell survival. This finding led to the proposal that DJ-1 acts as a novel regulator of PTEN. Our genetic and biochemical studies are consistent with this notion. It is not clear at this point how DJ-1A and the PI3K PTEN Akt-signaling pathway may interact. It is possible that the function of DJ-1 in regulating cellular ROS homeostasis or as a redox-sensitive molecular chaperone may facilitate PI3K PTEN Akt signaling, because many signal transduction pathways are known to be sensitive to cellular ROS levels or require chaperone activities (33, 34), and modulation of PTEN activity by ROS has been reported before (35). Alternatively, the genetic interaction between DJ-1A and PI3K-signaling pathway may be mediated by a direct role of PI3K signaling in cellular defense against ROS accumulation and related damages. Our data are consistent with both possibilities. Given that hyperactivation of DJ-1 could be oncogenic, whereas its deficiency leads to neuronal dysfunction and degeneration, future studies aimed at understanding the mechanisms by which DJ-1 and PI3K PTEN Akt pathway interact will have far-reaching implications for understanding disease mechanisms and developing therapeutic strategies.

Oxidative stress and mitochondrial dysfunction are being increasingly recognized as common pathological features of neurodegenerative diseases including PD and Alzheimer's disease (2, 36). Previous genetic studies in *Drosophila* and mice have implicated Parkin, an E3 ubiquitin ligase associated with autosomal recessive juvenile parkinsonism, in these processes (37–40). In flies and mice, *parkin* mutants show defects in mitochondrial function and oxidative stress response. Like DJ-1, loss of *Drosophila* Parkin function also affects the viability of mutant animals. This result contrasts with the situation in mammals where loss of DJ-1 or Parkin is nonlethal. The differential effects on the viability of humans and flies are probably caused by fundamental differences in the antioxidant defense systems of these two species (41). The exact cellular mechanism by which Parkin dysfunction leads to susceptibility to oxidative stress and cell death remains to be established. Our finding that, similar to DJ-1A inactivation, inhibition of *parkin* also leads to impairment of PI3K Akt signaling implicates these two genes in a common pathway that promotes neuronal survival. We speculate that impairment of PI3K Akt signaling may be a common feature of familial as well as sporadic PD cases and that manipulation of this signaling pathway may provide a rational strategy for the therapeutic intervention of PD.

We are grateful to Drs. Morris Birnbaum (University of Pennsylvania, Philadelphia), Mel Feany (Harvard University, Boston), Ernst Hafen (University of Zurich, Zurich), Raj Sohal (University of Southern California, Los Angeles), Bertrand Mollereau (The Rockefeller University, New York), Hermann Steller (The Rockefeller University), Tian Xu (Yale University, New Haven, CT), and the Bloomington *Drosophila* Stock Center for fly stocks; Dr. Kazuaki Yoshikawa for his generous support; the Center for Research and Education of Osaka University School of Medicine for help with SEM and eye sectioning; Dr. Su Guo for reading the manuscripts; Dr. Ting-ting Huang for help with H_2O_2 assay; and Dr. Kyung-Tai Min for communicating unpublished results. Special thanks go to Jennifer Quach and Yali Zhang for excellent technical support and members of the B.L. laboratory for discussions. This work was supported by the McKnight, Beckman, and Sloan Foundations (to B.L.).

1. Dunnett, S. B. & Bjorklund, A. (1999) *Nature* **399,** A32–A39.
2. Dawson, T. M. & Dawson, V. L. (2003) *Science* **302,** 819–822.
3. Shen, J. & Cookson, M. R. (2004) *Neuron* **43,** 301–304.
4. Nagakubo, D., Taira, T., Kitaura, H., Ikeda, M., Tamai, K., Iguchi-Ariga, S. M. & Ariga, H. (1997) *Biochem. Biophys. Res. Commun.* **231,** 509–513.
5. Hod, Y., Pentyala, S. N., Whyard, T. C. & El-Maghrabi, M. R. (1999) *J. Cell Biochem.* **72,** 435–444.
6. Takahashi, K., Taira, T., Niki, T., Seino, C., Iguchi-Ariga, S. M. & Ariga, H. (2001) *J. Biol. Chem.* **276,** 37556–37563.
7. Canet-Aviles, R. M., Wilson, M. A., Miller, D. W., Ahmad, R., McLendon, C., Bandyopadhyay, S., Baptista, M. J., Ringe, D., Petsko, G. A. & Cookson, M. R. (2004) *Proc. Natl. Acad. Sci. USA* **101,** 9103–9108.
8. Mitsumoto, A. & Nakagawa, Y. (2001) *Free Radical Res.* **35,** 885–893.
9. Mitsumoto, A., Nakagawa, Y., Takeuchi, A., Okawa, K., Iwamatsu, A. & Takanezawa, Y. (2001) *Free Radical Res.* **35,** 301–310.
10. Kinumi, T., Kimata, J., Taira, T., Ariga, H. & Niki, E. (2004) *Biochem. Biophys. Res. Commun.* **317,** 722–728.
11. Yokota, T., Sugawara, K., Ito, K., Takahashi, R., Ariga, H. & Mizusawa, H. (2003) *Biochem. Biophys. Res. Commun.* **312,** 1342–1348.
12. Goldberg, M. S., Pisani, A., Haburcak, M., Vortherms, T. A., Kitada, T., Costa, C., Tong, Y., Martella, G., Tscherter, A., Martins, A., *et al.* (2005) *Neuron* **45,** 489–496.
13. Kim, R. H., Smith, P. D., Aleyasin, H., Hayley, S., Mount, M. P., Pownall, S., Wakeham, A., You-Ten, A. J., Kalia, S. K., Horne, P., *et al.* (2005) *Proc. Natl. Acad. Sci. USA* **102,** 5215–5220.
14. Chen, L., Cagniard, B., Mathews, T., Jones, S., Koh, H. C., Ding, Y., Carvey, P. M., Ling, Z., Kang, U. J. & Zhuang, X. (2005) *J. Biol. Chem.* **280,** 21418–21426.
15. Kim, R. H., Peters, M., Jang, Y., Shi, W., Pintilie, M., Fletcher, G. C., DeLuca, C., Liepa, J., Zhou, L., Snow, B., *et al.* (2005) *Cancer Cell* **7,** 263–273.
16. Verdu, J., Buratovich, M. A., Wilder, E. L. & Birnbaum, M. J. (1999) *Nat. Cell Biol.* **1,** 500–506.
17. Leevers, S. J., Weinkove, D., MacDougall, L. K., Hafen, E. & Waterfield, M. D. (1996) *EMBO J.* **15,** 6584–6594.
18. Huang, H., Potter, C. J., Tao, W., Li, D. M., Brogiolo, W., Hafen, E., Sun, H. & Xu, T. (1999) *Development (Cambridge, U.K.)* **126,** 5365–5372.
19. Wittmann, C. W., Wszolek, M. F., Shulman, J. M., Salvaterra, P. M., Lewis, J., Hutton, M. & Feany, M. B. (2001) *Science* **293,** 711–714.
20. Kalidas, S. & Smith, D. P. (2002) *Neuron* **33,** 177–184.
21. Yang, Y., Nishimura, I., Imai, Y., Takahashi, R. & Lu, B. (2003) *Neuron* **37,** 911–924.
22. Nishimura, I., Yang, Y. & Lu, B. (2004) *Cell* **116,** 671–682.
23. Ito, S., Kato, T. & Fujita, K. (1988) *Biochem. Pharmacol.* **37,** 1707–1710.
24. Beal, M. F., Kowall, N. W., Swartz, K. J. & Ferrante, R. J. (1990) *Neurosci. Lett.* **108,** 36–42.
25. Tao, X. & Tong, L. (2003) *J. Biol. Chem.* **278,** 31372–31379.
26. Feany, M. B. & Bender, W. W. (2000) *Nature* **404,** 394–398.
27. Taira, T., Saito, Y., Niki, T., Iguchi-Ariga, S. M., Takahashi, K. & Ariga, H. (2004) *EMBO Rep.* **5,** 213–218.
28. Bergmann, A., Agapite, J., McCall, K. & Steller, H. (1998) *Cell* **95,** 331–341.
29. Kuranaga, E., Kanuka, H., Igaki, T., Sawamoto, K., Ichijo, H., Okano, H. & Miura, M. (2002) *Nat. Cell Biol.* **4,** 705–710.
30. Martinat, C., Shendelman, S., Jonason, A., Leete, T., Beal, M. F., Yang, L., Floss, T. & Abeliovich, A. (2004) *PloS Biol.* **2,** e327.
31. Jang, H. H., Lee, K. O., Chi, Y. H., Jung, B. G., Park, S. K., Park, J. H., Lee, J. R., Lee, S. S., Moon, J. C., Yun, J. W., *et al.* (2004) *Cell* **117,** 625–635.
32. Shendelman, S., Jonason, A., Martinat, C., Leete, T. & Abeliovich, A. (2004) *PLoS Biol.* **2,** e362.
33. Shibata, Y., Branicky, R., Landaverde, I. O. & Hekimi, S. (2003) *Science* **302,** 1779–1782.
34. Morey, M., Serras, F., Baguna, J., Hafen, E. & Corominas, M. (2001) *Dev. Biol.* **238,** 145–156.
35. Leslie, N. R., Bennett, D., Lindsay, Y. E., Stewart, H., Gray, A. & Downes, C. P. (2003) *EMBO J.* **22,** 5501–5510.
36. Albers, D. S. & Beal, M. F. (2000) *J. Neural Transm.* **59,** Suppl., 133–154.
37. Kitada, T., Asakawa, S., Hattori, N., Matsumine, H., Yamamura, Y., Minoshima, S., Yokochi, M., Mizuno, Y. & Shimizu, N. (1998) *Nature* **392,** 605–608.
38. Greene, J. C., Whitworth, A. J., Kuo, I., Andrews, L. A., Feany, M. B. & Pallanck, L. J. (2003) *Proc. Natl. Acad. Sci. USA* **100,** 4078–4083.
39. Pesah, Y., Pham, T., Burgess, H., Middlebrooks, B., Verstreken, P., Zhou, Y., Harding, M., Bellen, H. & Mardon, G. (2004) *Development (Cambridge, U.K.)* **131,** 2183–2194.
40. Palacino, J. J., Sagi, D., Goldberg, M. S., Krauss, S., Motz, C., Klose, J. & Shen, J. (2004) *J. Biol. Chem.* **279,** 18614–18622.
41. Kanzok, S. M., Fechner, A., Bauer, H., Ulschmid, J. K., Muller, H. M., Botella-Munoz, J., Schneuwly, S., Schirmer, R. & Becker, K. (2001) *Science* **291,** 643–646.

nature neuroscience

Chromogranin-mediated secretion of mutant superoxide dismutase proteins linked to amyotrophic lateral sclerosis

Makoto Urushitani[1], Attila Sik[2], Takashi Sakurai[3], Nobuyuki Nukina[3], Ryosuke Takahashi[4] & Jean-Pierre Julien[1]

Here we report that chromogranins, components of neurosecretory vesicles, interact with mutant forms of superoxide dismutase (SOD1) that are linked to amyotrophic lateral sclerosis (ALS), but not with wild-type SOD1. This interaction was confirmed by yeast two-hybrid screen and by co-immunoprecipitation assays using either lysates from Neuro2a cells coexpressing chromogranins and SOD1 mutants or lysates from spinal cord of ALS mice. Confocal and immunoelectron microscopy revealed a partial colocalization of mutant SOD1 with chromogranins in spinal cord of ALS mice. Mutant SOD1 was also found in immuno-isolated trans-Golgi network and in microsome preparations, suggesting that it can be secreted. Indeed we report evidence that chromogranins may act as chaperone-like proteins to promote secretion of SOD1 mutants. From these results, and our finding that extracellular mutant SOD1 can trigger microgliosis and neuronal death, we propose a new ALS pathogenic model based on the toxicity of secreted SOD1 mutants.

ALS is a progressive adult-onset neurodegenerative disorder that affects primarily motor neurons in the brain and spinal cord. The disease typically begins locally and spreads, leading to paralysis and death within 3–5 years. Approximately 10% of ALS cases are familial and 90% are sporadic. Mutations in the genes encoding SOD1 (ref. 1) are involved in 20% of familial ALS cases.

Despite a decade of investigation on familial ALS caused by missense mutations in the *SOD1* gene, the mechanism of toxicity to motor neurons has remained elusive. Transgenic mice expressing mutant forms of SOD1 develop motor neuron disease resembling ALS through a gain of unidentified deleterious properties[2]. Eliminating the copper chaperone for SOD1 does not diminish the toxicity of mutant SOD1 in mice[3], and mutations that disrupt the copper-binding site of mutant SOD1 do not suppress toxicity[4]. Thus, it is now thought that the toxicity of mutant SOD1 is not related to aberrant copper-mediated catalysis but rather to the propensity of the abnormal protein to aggregate, a phenomenon common to many neurodegenerative diseases[5,6]. Cell culture studies have shown that the mutant SOD1 proteins induce oxidative stress[7,8], form aggregates[9,10] and impair proteasomal function[11].

Notably, recent lines of evidence indicate that the toxicity of SOD1 mutants is non-cell-autonomous. The neuron-specific expression of mutant SOD1 does not provoke motor neuron disease[12,13]. Moreover, chimeric mouse studies with SOD1 mutants have demonstrated that neurodegeneration is delayed or eliminated when motor neurons expressing mutant SOD1 are surrounded by healthy wild-type cells[14]. Moreover, these studies show evidence of damage to wild-type motor neurons by surrounding cells expressing mutant SOD1. Such results emphasize the importance of a motor neuron milieu, but the mechanism by which the toxicity of mutant SOD1 may be transferred from one cell to another is still unclear[14].

So far, proteins known to interact with mutant forms of SOD1 but not with wild-type SOD1 have been implicated in protein refolding or proteasomal degradation (for example, heat-shock proteins Hsp40, Hsp/Hsc70 (refs. 15,16) and CHIP[16]). To search for more proteins that interact with mutant SOD1, we performed yeast two-hybrid screening of a cDNA library from the total spinal cord of presymptomatic transgenic mice expressing the G93A SOD1 mutation (in which a glycine residue is replaced by an alanine residue). We discovered that chromogranins are interacting partners with mutant forms of SOD1, but not wild-type SOD1. The chromogranins, namely chromogranin-A (CgA) and chromogranin-B (CgB), are soluble, acidic glycophosphoproteins and are major constituents of secretory large dense-core vesicles (LDCV) in neurons and endocrine cells. LDCV store neuropeptides and hormones and show regulated exocytosis upon appropriate cellular stimulation[17]. Chromogranins are transported in the trans-Golgi network (TGN) and translocate at the periphery in an actin-dependent manner during their maturation process[18]. Although the physiological functions of chromogranins are still unclear, previous reports have shown that their proteolytic products function as antibiotics, regulators of hormone release, controllers of intracellular Ca^{2+} concentration and protein sorting machineries[17]. The role of chromogranins in neurons is unknown. Both CgA and CgB proteins are transported in the rat sciatic

[1]Department of Anatomy and Physiology, Laval University, Centre de Recherche du Centre Hospitalier de l' Université Laval, 2705 boulevard Laurier, Sainte-Foy, Quebec G1V 4G2, Canada. [2]Department of Psychiatry, Centre de Recherche Université Laval Robert-Giffard, 2601 de la Canardiere, Quebec, Quebec G1J 2G3, Canada. [3]Laboratory for Structural Neuropathology and [4]Motor System Neurodegeneration, RIKEN Brain Science Institute, 2-1 Hirosawa, Wako, Saitama, 351-0198, Japan. Correspondence should be addressed to J.-P.J. (jean-pierre.julien@crchul.ulaval.ca).

Received 15 September; accepted 26 October; published online 20 December 2005; doi:10.1038/nn1603

nerve[19] and CgA is found in motor endplates in the diaphragm[20], suggesting a possible role in neurotransmission.

Previous evidence indicates that chromogranins are involved in neurodegenerative diseases. Immunohistochemical studies have revealed the presence of CgA or CgB in neuritic senile plaques of Alzheimer brains[21] and in prion protein deposits of Creutzfeldt-Jacob disease brains[22]. The staining pattern of CgA is also altered in motor neurons of people with sporadic ALS[23]. Importantly, there is evidence that CgA can activate microglia to produce various pro-inflammatory molecules such as tumor necrosis factor-alpha (TNF-α), nitric oxide and potential neurotoxins including glutamate and cathepsin B[24–26].

Here we report that CgA and CgB, which are abundant proteins in motor neurons and interneurons, may act as chaperone-like proteins to

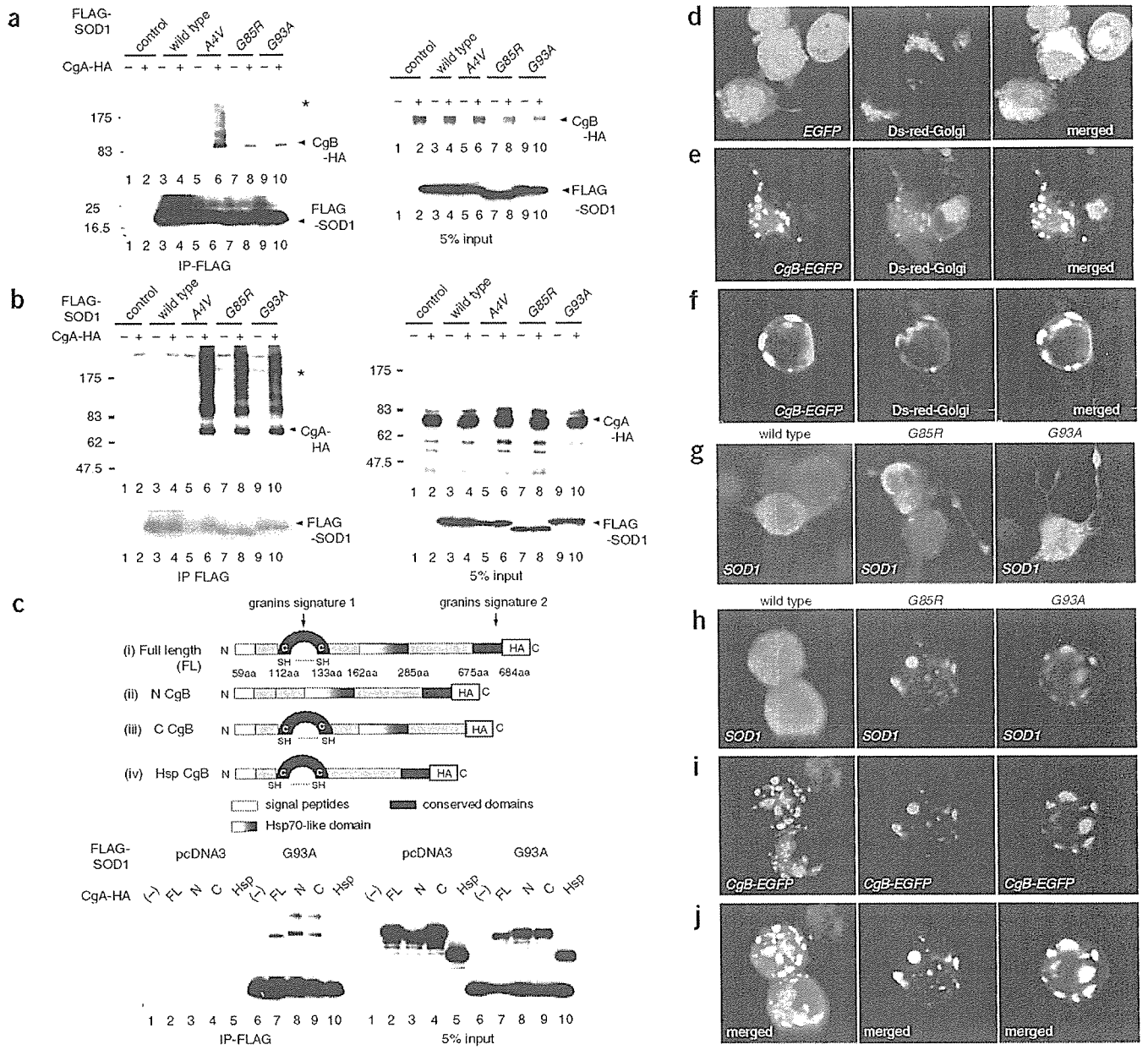

Figure 1 Selective interactions of chromogranins with mutant SOD1 species but not with wild-type SOD1. (**a**,**b**) Chromogranins interact with mutant SOD1 in cultured cells. Neuro2a cells were transiently transfected with FLAG-tagged human *SOD1* (wild-type, A4V, G85R or G93A) and HA-tagged mouse CgB (**a**) or CgA (**b**). Immunoprecipitates with anti-FLAG affinity gel (IP-FLAG) and total cell lysates (5% input) were analyzed by western blotting using antibodies to SOD1 or HA. Note that both CgB and CgA immunoprecipitated with mutant SOD1 to yield high molecular weight species (asterisk). (**c**) An Hsp70-like domain in CgB interacts with mutant SOD1. Schematic representation of full-length (FL) or deletion mutants (N terminus (ΔN), C terminus (ΔC) or Hsp70-like domain (ΔHsp)) of CgB (top). Total cell lysates and immunoprecipitates from Neuro2a cells transfected with *FLAG-SOD1* or full-length *CgB* (FL) or its deletion mutants (ΔN, ΔC, ΔHsp) were analyzed by western blotting using the same antibodies (bottom). (**d–f**) Localization of CgB in the TGN of transfected Neuro2a cells. Images show live cells from confocal laser microscope of Neuro2a cells transfected with a plasmid encoding Ds-Red and a Golgi marker (*Ds-Red-Golgi*, middle) and EGFP (**d**) or EGFP-fused CgB (*CgB-EGFP*, **e** and **f**). (**g–j**) Overexpressed SOD1 mutants localized with CgB in the TGN of Neuro2a cells. Neuro2a cells were transiently transfected with human SOD1 (wild-type, G85R and G93A) together with (**i–k**) or without (**h**) CgB-EGFP, and analyzed by immunocytochemistry using mouse monoclonal anti-SOD1.

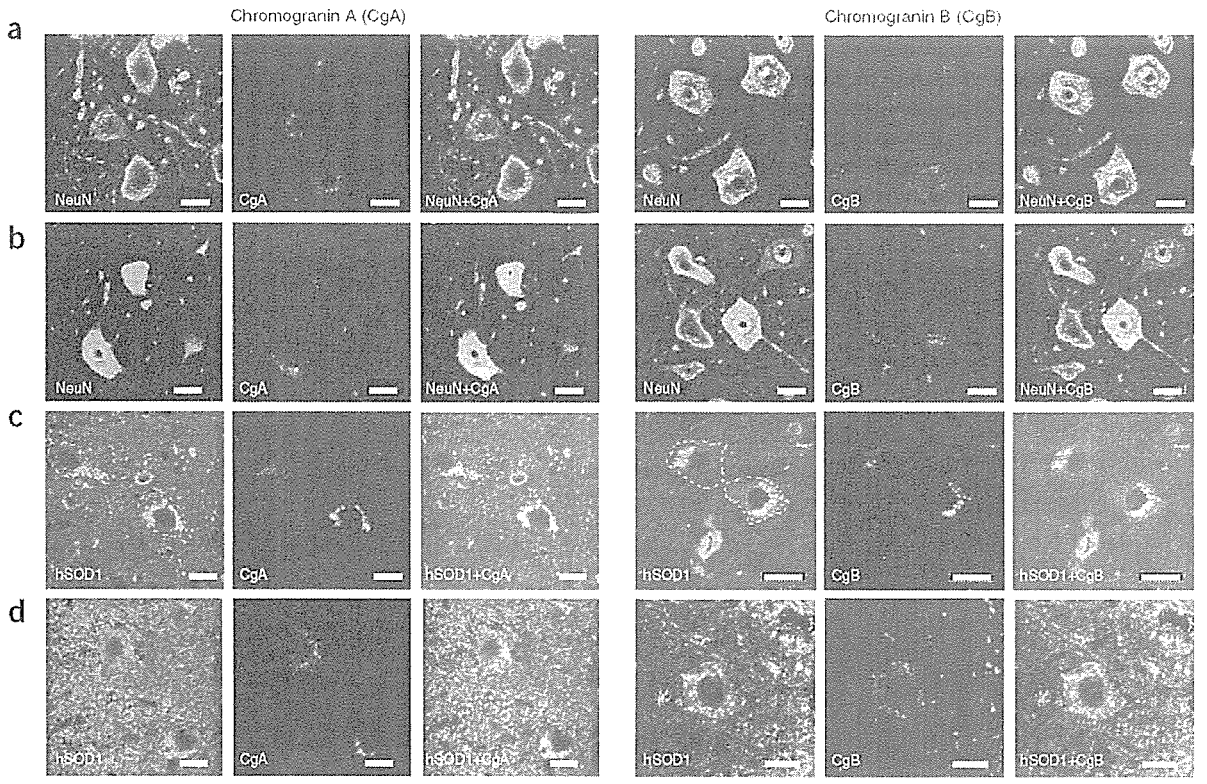

Figure 2 Expression pattern of chromogranins in *SOD1* transgenic mice. We used the lumbar spinal cords from (**a**) nontransgenic littermates, (**b**,**c**) transgenic mice at 7 months of age and (**d**) transgenic mice at 9 months of age. The transgenic mice expressed either G37R *SOD1* (**b**,**c**) or wild-type *SOD1* (**d**). The following combinations of antibody stains were used: (**a**,**b**) mouse monoclonal anti-NeuN plus rabbit polyclonal anti-CgA (left) or anti-CgB (right); (**c**,**d**) sheep polyclonal antibody specific to human SOD1 plus anti-CgA (left) or anti-CgB (right). In **c**, the dotted lines demarcate the cell body of motor neurons. Scale bars, 50 μm.

promote secretion of misfolded SOD1 mutants. Moreover, our results demonstrate that extracellular mutant SOD1 can induce microgliosis and motor neuron death, suggesting that the chromogranin-mediated secretion of mutant SOD1 proteins could be a pathogenic mechanism in ALS. This idea is consistent with findings that the disease is not strictly autonomous to motor neurons and that toxicity is transferable from one cell to another.

RESULTS

Interaction of CgA and CgB with mutant SOD1 in cultured cells

To identify new proteins that interact with mutant SOD1, we used a yeast two-hybrid approach to screen a cDNA library from the spinal cord of pre-symptomatic mice transgenic for human G93A *SOD1*, using monomeric LexA-human G93A SOD1 as bait. As expected, the majority of the 250 surviving clones expressed human SOD1 that can dimerize with the bait. However, we obtained one clone whose sequence corresponded to a partial mouse CgB sequence encoding 76 amino acids. A full-length mouse CgB clone was then isolated from a brain cDNA library of C57Bl/6 mice and used as bait in the yeast two-hybrid system to confirm a specific interaction of CgB with mutant SOD1, but not with wild-type SOD1 (data not shown). To further investigate the interaction of CgB with mutant forms of SOD1 in a mammalian cell system, we carried out transient coexpression assays with Neuro2a cells using plasmid vectors coding for CgB tagged with hemagglutinin (HA) at the carboxy (C) terminus and for various human SOD1 species tagged with FLAG at the amino (N) terminus. We tested various SOD1 mutants, including the A4V, G85R and G93A mutants, to confirm that chromogranins interact with misfolded SOD1 mutants in general, not just the G93A mutant. As shown in pull-down assays (**Fig. 1a**), CgB was co-immunoprecipitated with mutant forms of SOD1, but not with wild-type SOD1. Pull-down assays revealed that CgA, another member of the mouse chromogranin family, also associated with SOD1 mutants but not with wild-type SOD1 (**Fig. 1b**). Similar results were obtained with human chromogranins (data not shown).

CgA and CgB share two conserved domains near their N and C termini, named the granin domains. The N-terminal granin domain is implicated in a sorting mechanism[27], whereas the C-terminal granin domain is necessary for dimerization or tetramerization of chromogranins[28]. To determine the CgB region responsible for interaction with mutant SOD1, we constructed expression plasmids for CgB mutants lacking specific domains and transiently expressed them together with mutant SOD1 into Neuro2a cells (**Fig. 1c**, top). An immunoprecipitation experiment showed that CgB mutants with deleted granin domains (ΔN or ΔC) were still able to interact with mutant SOD1 (**Fig. 1c**, bottom). A search for sequence homologies revealed that both CgB and CgA contain internal sequences with homologies to the substrate-binding site of mammalian Hsp70 (**Supplementary Fig. 1** online). A CgB mutant lacking this internal region (ΔHsp) did not bind mutant SOD1, as determined by the pull-down assay (**Fig. 1c**). The presence of an Hsp70-like domain offers a reasonable explanation for the specific binding of chromogranins to misfolded SOD1 mutants and not to wild-type SOD1.

Confocal microscopy of transfected Neuro2a cells provided further evidence of interactions between SOD1 mutants and chromogranins. Transfection of a construct encoding CgB fused at the C terminus to

enhanced green fluorescent protein (EGFP) (*CgB-EGFP*) into Neuro2a cells showed CgB accumulation in the TGN, as indicated by colocalization with Ds-Red fused to the Golgi-targeting human β1,4-galactoysltransferase (Ds-Red-Golgi) (**Fig. 1d–f**). Unlike chromogranins, SOD1 is a cytosolic protein without signal peptide and it is synthesized in free ribosomes. As expected, wild-type SOD1 yielded a cytosolic distribution when overexpressed in Neuro2a cells, and the expression of CgB had no effect on its distribution (**Fig. 1g–j**, left). In contrast, the subcellular distribution of mutant SOD1 species (G85R or G93A) was altered by the overexpression of CgB. A total colocalization of mutant SOD1 with CgB was observed in roughly 10% of doubly transfected Neuro2a cells (**Fig. 1g–j**, middle and right). These results indicate that CgB can influence the subcellular distribution of SOD1 mutants under the condition of overexpression in cultured cells.

Colocalization of mutant SOD1 and CgA/B *in vivo*

We confirmed by *in situ* hybridization that CgA and CgB are expressed throughout the gray matter of spinal cord in mice, in motor neurons, interneurons and dorsal neurons. Immunohistochemistry showed that both CgA and CgB are more predominantly detected in dorsal neurons and interneurons than in motor neurons (**Supplementary Fig. 2** online), which is consistent with previous reports[29,30].

Immunofluorescence microscopy showed that CgA and CgB are located in perinuclear vesicles in the spinal motor neurons of normal mice stained by anti-NeuN antibody (**Fig. 2a**). In presymptomatic *G37R SOD1* mice (7 months old), perinuclear vesicles labeled by antibody to CgA or CgB were deformed and fused together (**Fig. 2b**), possibly reflecting damage to the Golgi apparatus[31]. We also detected partial colocalization of mutant SOD1 with CgA and CgB in irregular and large vesicular structures of spinal neurons from *G37R SOD1* transgenic mice (**Fig. 2c**). In the *SOD1* (wild-type) transgenic mice, the distribution patterns of CgA and CgB were similar to those of nontransgenic mice with no obvious colocalization between wild-type SOD1 and chromogranins (**Fig. 2d**).

To confirm the distribution of mutant SOD1 in the endoplasmic reticulum (ER)-Golgi system, we carried out subcellular fractionation of spinal cord lysates from transgenic mice expressing wild-type SOD1 or G37R SOD1 at different ages. Western blot analysis clearly demonstrated that mutant SOD1 was recovered in both heavy and light membrane fractions containing mitochondria and microsomes (**Fig. 3a**). The calculation from the densitometric value of SOD1 monomer revealed that, in the preclinical stage (6 months old), 23.6% of G37R SOD1 was found in heavy membrane fractions, and 4.2% in light membrane fractions. For wild-type SOD1, 13.4% was found in heavy membrane fractions and 1.91% in light membrane fractions. After paralysis, 6.46% of monomeric G37R SOD1 accumulated in the light membrane

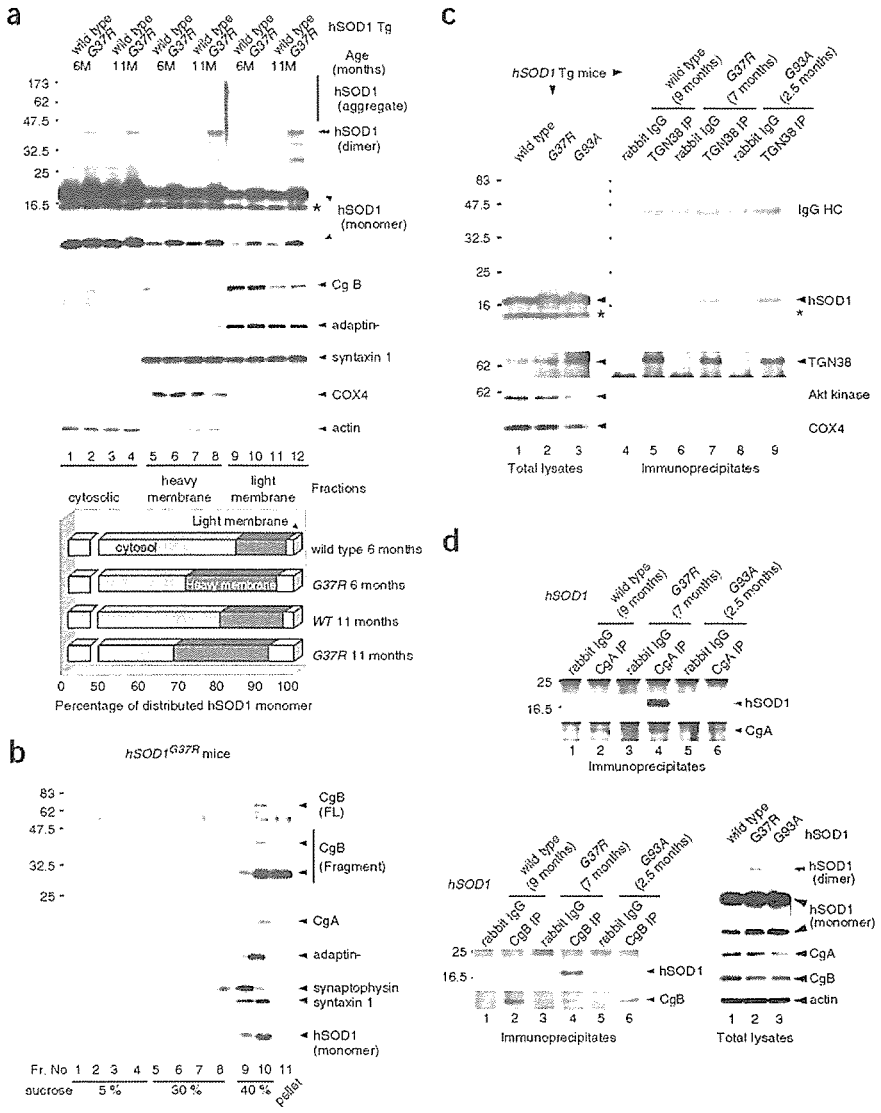

Figure 3 SOD1 mutants in spinal cord of ALS mice accumulate in TGN and co-immunoprecipitate with chromogranins. (**a**) G37R SOD1 accumulated in both heavy and light membrane fractions. Subcellularly fractionated proteins from spinal cord of wild-type and G37R *SOD1* transgenic mice (6 and 11 months old) was analyzed by western blotting using antibodies specific to human SOD1, CgB, adaptin-γ, syntaxin-1, COX4 and actin. Asterisk indicates endogenous mouse SOD1. The percentage of monomeric human SOD1 in each fraction was presented from the densitometric value of monomeric SOD1 in the cytosolic, heavy and light membrane fractions that was standardized by actin, COX4 and syntaxin-1, respectively (bottom). (**b**) Fractionation of microsome components by sucrose density-gradient ultracentrifugation showing that G37R SOD1 co-distributed with CgA, CgB, adaptin-γ and syntaxin-1. The light membrane fraction from spinal cord of G37R *SOD1* transgenic mice (7 months old) was analyzed. (**c**) Distribution of SOD1 mutants in the TGN. The spinal cord lysates from transgenic mice expressing human wild-type *SOD1* (9 months), G37R (7 months) or G93A (3 months) *SOD1* were immunoprecipitated with rabbit polyclonal anti-TGN38 preincubated with Protein G magnetic beads. The total tissue lysates and immunoprecipitates were analyzed by western blotting with antibodies to human SOD1, TGN38, Akt kinase and COX4. (**d**) Pull-down assay showing that CgA and CgB interacted with mutant SOD1 but not wild-type SOD1 in human SOD1 transgenic mice (wild-type, G37R and G93A). Spinal cord lysates were immunoprecipitated with anti-CgA or anti-CgB, which was analyzed using antibody to human SOD1.

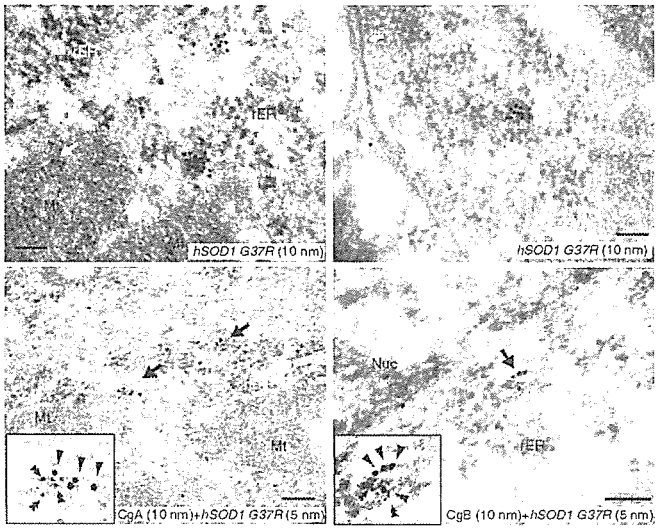

Figure 4 Immunoelectron microscopy reveals partial colocalization of G37R SOD1 with chromogranins. Ultra-thin sections of spinal anterior horn from G37R *SOD1* mice (7 months old) were incubated with sheep polyclonal antibody to human SOD1 alone (top panels), or together with rabbit polyclonal antibody to CgA or CgB (lower left or right, respectively). For secondary antibody, we used 10-nm (top panels) or 5-nm (bottom panels) immunogold-conjugated anti-sheep IgG and 10-nm immunogold-conjugated anti-rabbit IgG antibodies. In rough ER, 10-nm clusters of immuno-gold particles were frequently detected (arrowheads). G37R SOD1 was occasionally detected in mitochondria (arrow, top-left), or in a vesicle (arrowhead, top-right) close to the plasma membrane (arrows, top-right). Double-staining revealed frequent 10-nm clusters of CgA or CgB (arrowheads, bottom left or right) and 5-nm gold particles (hSOD1, double arrowheads, bottom panels). Scale bars, 100 nm.

fractions, whereas only 2.61% of wild-type SOD1 accumulated there (**Fig. 3a**, bottom). Furthermore, G37R SOD1 but not wild-type SOD1 formed non-native dimers and high molecular aggregates in the membrane fractions in an age-dependent manner. To further clarify the distribution of mutant SOD1 in the transport vesicles, we performed sucrose density gradient ultracentrifugation of post-mitochondrial membrane fractions using spinal cord extract from presymptomatic G37R *SOD1* transgenic mice at 7 months old. Western blotting revealed that mutant SOD1 had a distribution pattern similar to chromogranins, the trans-Golgi marker adaptin-γ and the SNARE protein syntaxin-1, but different from the pattern of synaptophysin (**Fig. 3b**).

To further confirm the distribution of mutant SOD1 species in a secretory pathway, we purified TGN from the spinal cord lysates of *SOD1* (wild-type), G37R *SOD1* and G93A *SOD1* transgenic mice by an immuno-isolation technique using anti-TGN38 antibody bound to protein G–coated magnetic beads. Anti-TGN38 is an affinity-purified polyclonal antibody specific to a 23-amino acid peptide corresponding to the cytosolic domain of rat and mouse TGN38 protein. Western analysis of the immunoprecipitates demonstrated that both G37R and G93A SOD1 co-precipitated with TGN38, indicating that mutant SOD1 is distributed in the TGN (**Fig. 3c**). Note that the wild-type SOD1 was also detectable in the TGN preparation, albeit at lower levels than mutant SOD1.

Further evidence for the specific interaction of CgA or CgB with mutant SOD1 proteins came from co-immunoprecipitation experiments using spinal cord lysates of transgenic mice. We found that rabbit polyclonal anti-CgA or anti-CgB antibody was able to pull down both G37R and G93A SOD1 mutants but not wild-type SOD1 (**Fig. 3d**). It should be noted that a non-native dimer of G37R SOD1 was more apparent than G93A SOD1 (double arrowhead), corresponding to the larger amount of co-immunoprecipitated G37R SOD1 than G93A SOD1.

To further investigate the distribution and colocalization of mutant SOD1 and chromogranins, we examined spinal cord sections from *SOD1* (wild-type) and G37R *SOD1* transgenic mice (7 months old) using immunoelectron microscopy. Mutant SOD1 protein was observed as small clusters of gold particles in the cytosol (**Supplementary Fig. 3** online), rough ER (arrowheads in **Fig. 4**, top-left), smooth ER and Golgi (**Supplementary Fig. 3**), and occasionally it was observed in mitochondria (arrow in **Fig. 4**, top-left) and transport vesicles (**Fig. 4**, top-right). Moreover, the double immunohistochemistry using secondary antibodies conjugated with different gold particles (5 nm or 10 nm) provided frequent detection of cluster complexes

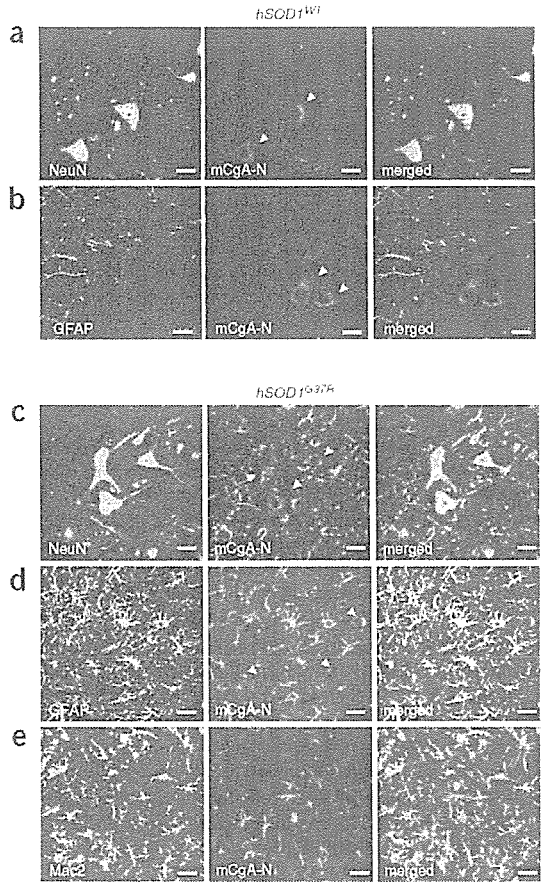

Figure 5 CgA is expressed in reactive astrocytes of spinal anterior horn from mutant *SOD1* transgenic mice. Double immunofluorescent experiments show the colocalization of CgA and GFAP in the spinal cord of transgenic mice carrying mutant *SOD1*, but not those carrying wild-type *SOD1*. (**a**,**b**) In wild-type *SOD1* mice, CgA was expressed only in the neurons labeled by anti-NeuN (**a**, mouse monoclonal), but not in reactive astrocytes labeled by anti-GFAP (**b**, mouse monoclonal). In G37R *SOD1* mice, in addition to the neuronal expression (**c**), CgA was also detected in reactive astrocytes (**d**), but not in the active microglial cells labeled by anti-Mac2 (**e**, rat monoclonal). Arrowheads and arrows, respectively, indicate neurons and astrocytes stained with anti-mCgA-N′. Left panels represent merged images from left and middle panels. Scale bars, 50 μm. Images show a representative sample from one of at least three independent experiments.

comprising SOD1 and chromogranins (**Fig. 4**; CgA bottom left, CgB bottom right). This colocalization was observed in rough ER, transport vesicles and granule-like structures. In contrast, wild-type SOD1 was chiefly located in the cytosol and occasionally in mitochondria and luminal structures including smooth and rough ER. The gold particles for wild-type human SOD1 tended to be singular or doublets, whereas clusters for G37R SOD comprised five to ten gold particles (**Supplementary Fig. 3**). No significant colocalization of wild-type SOD1 and chromogranins was detected. These findings confirm that mutant SOD1 can be recruited into the ER-Golgi pathway and interact with chromogranins.

Expression of CgA in reactive astrocytes in ALS mice

CgA is implicated in several neurodegenerative diseases including Alzheimer disease[21] and prion disease[22]. The N-terminal bioactive peptide of CgA, vasostatin, is implicated in microglial activation[24,32]. To investigate the distribution of proinflammatory fragments of CgA in the mutant *SOD1* transgenic mice, we raised a rabbit polyclonal antibody specific to the N-terminal peptide (16 amino acids) of the mature mouse CgA (anti-mCgA-N′).

Western analysis showed that anti-mCgA-N′ specifically recognized mouse CgA tagged by HA in the transfected COS-7 cells. Moreover, this antibody reacts with mouse CgA, but not with human CgA (**Supplementary Fig. 4** online). In transgenic mice overexpressing wild-type SOD1 (9 months old), immunofluorescence using anti-mCgA-N′ showed CgA detection predominantly in neurons co-stained with anti-NeuN (**Fig. 5a**) and rarely in astrocytes labeled by antibody specific to glial fibrillary acidic protein (anti-GFAP; **Fig. 5b**). In contrast, prominent anti-mCgA-N′ immunoreactivity was observed in reactive astrocytes of ventral horn in presymptomatic G37R *SOD1* mice (**Fig. 5c–e**, 8 months old) and G93A *SOD1* mice (**Supplementary Fig. 5** online, 80 d old). CgA also localized in neurons (**Fig. 5c**) but not in Mac2-labeled microglia (**Fig. 5e**) of G37R *SOD1* mice. Pre-incubation with the peptide antigen completely eliminated the signal (data not shown). These results suggest that CgA may be involved in the disease progression concomitant with astrocytosis.

CgA and CgB promote secretion of mutant SOD1

The combined microscopy and immunoprecipitation data presented above provide compelling evidence for the selective colocalization of

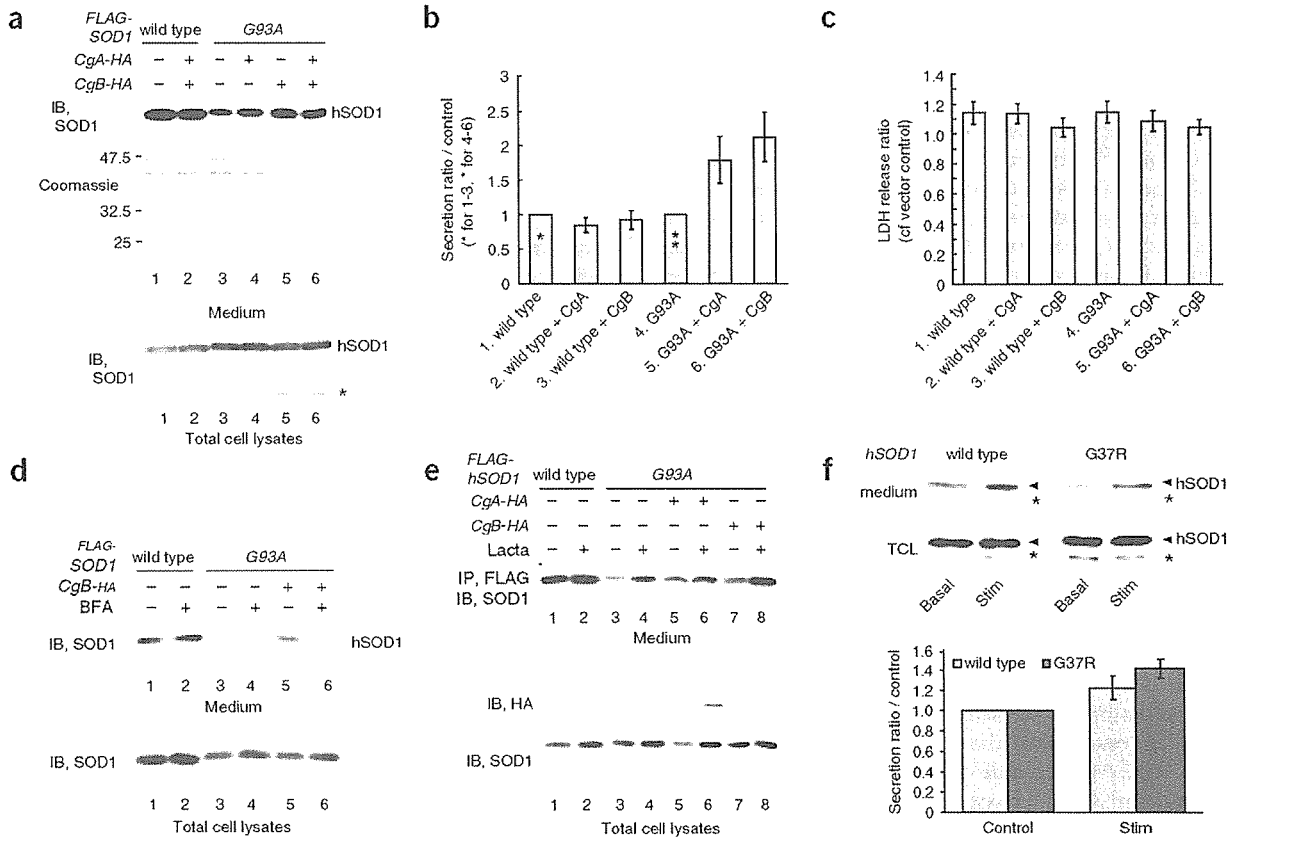

Figure 6 Chromogranins promote selective secretion of misfolded mutant SOD1. (**a**) CgA and CgB promoted specific secretion of mutant SOD1 in non-neurosecretory cells. COS-7 cells transfected with *FLAG-SOD1* (wild-type or G93A) and *CgA-HA* or *CgB-HA* were incubated in stimulation buffer. Medium was concentrated and analyzed by western blotting using SOD1-specific antibody. The SDS-PAGE gel was stained by Coomassie brilliant blue (Coomassie). Asterisk indicates endogenous SOD1. IB, immunoblot. (**b**) Densitometry of the secreted human SOD1 from the western blots. The values (mean ± s.e.m., $n = 3$) represent the ratio compared to control (lane 1 = control for wild-type (asterisk) and lane 4 = control for G93A SOD1 (double asterisks)). (**c**) LDH release assay demonstrating that transfection experiments did not provoke cell leakage. Medium was assayed 24 h after transfection. Value represents LDH release ratio compared with vector control (*pcDNA3*). Data are mean ± s.e.m. ($n = 3$). (**d**) Brefeldin A (BFA) inhibited chromogranin-mediated secretion of mutant SOD1. COS-7 cells transfected with FLAG-*SOD1* (wild-type or G93A) with or without CgB-HA were treated with 5 μM BFA for 1 h before exposure to stimulation buffer. (**e**) Effect of proteasomal inhibitor on mutant SOD1 secretion. Transfected NIH3T3 cells were treated with lactacystin for 20 h before the secretion assay. (**f**) Both wild-type and G37R SOD1 were secreted from embryonic spinal cord cultures from human SOD1 transgenic mice. Primary cultures were treated with basal or stimulation buffer for 15 min. Asterisks indicate endogenous mouse SOD1. Data given as ratio of secreted SOD1 from treated samples to that in basal-buffer samples (mean ± s.e.m., $n = 4$).

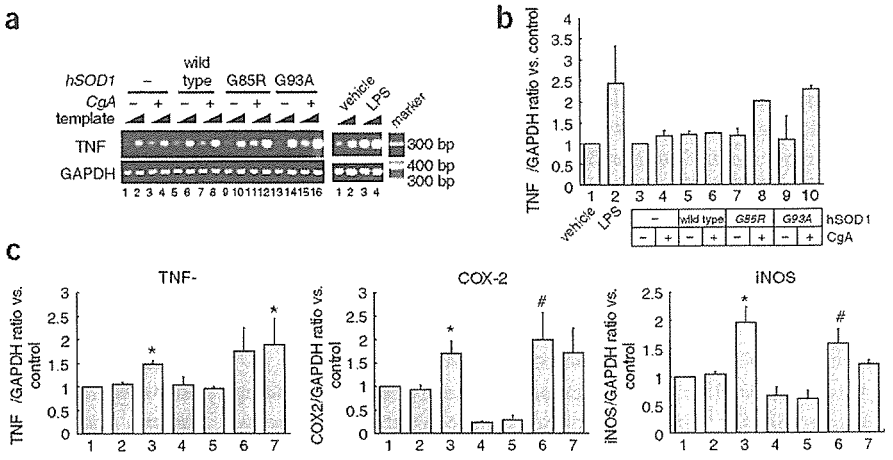

Figure 7 Activation of microglia by extracellular mutant SOD1. (**a**,**b**) Activation of microglial cell-line BV2 after treatment with conditioned medium from Neuro2a cells co-transfected with CgA and *SOD1* mutants (G85R or G93A). (**a**) RT-PCR study of TNF-α and GAPDH. For control, Neuro2a cells were treated with lipopolysaccharide (LPS). Notably, there was no microglial activation with medium from cells co-transfected with *CgA* and wild-type *SOD1*. Templates were examined at two different concentrations (1:10 diluted and original). (**b**) Each densitometric value was normalized with GAPDH and averaged from results of two different concentrations of templates. Each value represents a ratio compared to control lanes (bar 1 is the control for bar 2, and bar 3 is the control for 4–10), expressed as mean ± s.e.m. (**c**) Direct effect of mutant SOD1 on microglial activation. BV2 cells were treated with recombinant CgA (1 μg ml $^{-1}$), human SOD1 (wild-type or G93A, 2 μg ml $^{-1}$ each) or LPS (10 μg ml $^{-1}$) as a positive control for 18 h, as shown in the bottom box. Semi-quantitative RT-PCR was performed in the same manner as in **a**. Each densitometric value was normalized by GAPDH and an expression ratio was obtained by comparison with control (bar 1 in each graph). The ratio was averaged from three experiments and expressed as mean ± s.e.m. $^{*}P < 0.05$ versus sham treatment (lane 1). $^{\#}P < 0.05$ versus wild-type SOD1 treatment (lane 4) assessed by analysis of variance (ANOVA).

mutant SOD1 with chromogranins in mouse models of ALS. These results prompted us to investigate whether mutant SOD1 molecules were secreted together with chromogranins. We conducted secretion experiments using nongranular COS-7 cells that are lacking endogenous chromogranins[33]. Expression plasmids coding for FLAG-tagged SOD1 (wild-type or G93A mutant) and HA-tagged mouse CgA or CgB were transiently co-transfected in COS-7 cells. Both wild-type and G93A mutant SOD1 were detected by western analysis in the control medium after a 15-min incubation. Moreover, treatment with stimulation buffer containing 2-mM $BaCl_2$ and 50 mM KCl increased the amount of both wild-type and mutant SOD1 in the medium 1.2-fold compared with control buffer (data not shown). These data imply the existence of constitutive and regulatory secretory pathways for SOD1 in these cells. It is noteworthy that both CgA and CgB promoted secretion of G93A SOD1, whereas secretion of wild-type SOD1 was not affected by CgA or CgB (**Fig. 6a,b**). Judging from the amount of lactate dehydrogenase (LDH) released, the effects of chromogranins on secretion of mutant SOD1 did not result from cell death or membrane disintegration caused by overexpression (**Fig. 6c**). We also examined the effect of Brefeldin A (BFA) on SOD1 secretion to further address the involvement of the ER-Golgi network. In COS-7 cells, BFA did not reduce the secretion of either mutant or wild-type SOD1 in absence of CgB (**Fig. 6d**, lanes 2 and 5). BFA did, however, inhibit the CgB-mediated secretion of mutant SOD1 (**Fig. 6d**, lanes 7 and 8). This suggests that CgB contributes to the secretion of mutant SOD1 proteins through the TGN. We conclude that chromogranins promote the secretion of mutant SOD1, but not of wild-type SOD1.

Proteasome inhibition enhances secretion of mutant SOD1

Because previous studies showed an impairment of proteasomal activity in cells expressing mutant SOD1[11], we examined the effect of a proteasome inhibitor on the secretion of human SOD1 species in non-granular NIH3T3 cells. The treatment of transfected NIH3T3 cells with a specific proteasome inhibitor, lactacystin (5 μM), enhanced the secretion of mutant SOD1 in the presence or absence of chromogranins (**Fig. 6e**).

SOD1 secretion from spinal cultures of SOD1 mouse embryo

Both wild-type and mutant SOD1 have been detected in the cerebrospinal fluid (CSF) of *SOD1* transgenic rats[34] and humans carrying a SOD1 mutation[35]. However, it is technically difficult to prove this finding in mice, because of the small space for CSF with high occurrence of contamination from the blood or tissues. We carried out spinal cord cultures from *SOD1* transgenic mice to confirm that SOD1 can be secreted. Spinal cord cultures were prepared from E13 embryos and then analyzed after 14 d *in vitro*. Secretion analysis of the culture medium revealed that both wild-type and G37R SOD1 can be detected in basal secretion buffer. Exposure of the cells to stimulation buffer containing $BaCl_2$ (2 mM) and KCl (50 mM) for 15 min promoted the secretion of both wild-type and G37R SOD1, but more robustly in G37R (**Fig. 6f**). This result indicates that SOD1 can be secreted in both a constitutive and regulated manner.

Extracellular SOD1 mutants cause microgliosis and neuron death

There is evidence for involvement of CgA in microglial activation[32]. To examine the effects of secreted mutant SOD1 together with CgA on microglial activation, we treated BV2 microglial cells with conditioned medium from Neuro2a cells that were transfected with various human *SOD1* species (wild-type, G85R and G93A), with or without CgA. Semi-quantitative reverse-transcriptase PCR (RT-PCR) was performed using total RNA from BV2 cells to monitor expression of mRNA for proinflammatory molecules. RT-PCR results showed that the combination of mutant SOD1 and CgA resulted in a medium that induced TNF-α expression in BV2 cells (**Fig. 7a,b**).

To investigate whether extracellular SOD1 mutants activate microglia, we exposed the BV2 cells to recombinant human SOD1 or CgA (extracellular) to determine whether microglial activation was mediated directly by these molecules. The results showed that extracellular mutant G93A SOD1 with or without CgA induced BV2 cells to produce TNF-α, cyclooxygenase-2 (COX-2) and inducible nitric oxide synthase (iNOS) (**Fig. 7c**). In contrast to mutant SOD1, the recombinant wild-type SOD1 caused suppression of microglial activation, which is in agreement with a protective role for secreted wild-type SOD1 as recently suggested[35].

We further investigated the effects of extracellular SOD1 (wild-type and G93A) and CgA proteins using primary spinal cord cultures derived from E13 mouse embryos. Spinal cord cultures at 14 d after plating were exposed to these recombinant proteins or to lipopolysaccharide (LPS) for 24 h. Treatment of the cultures with CgA and/or

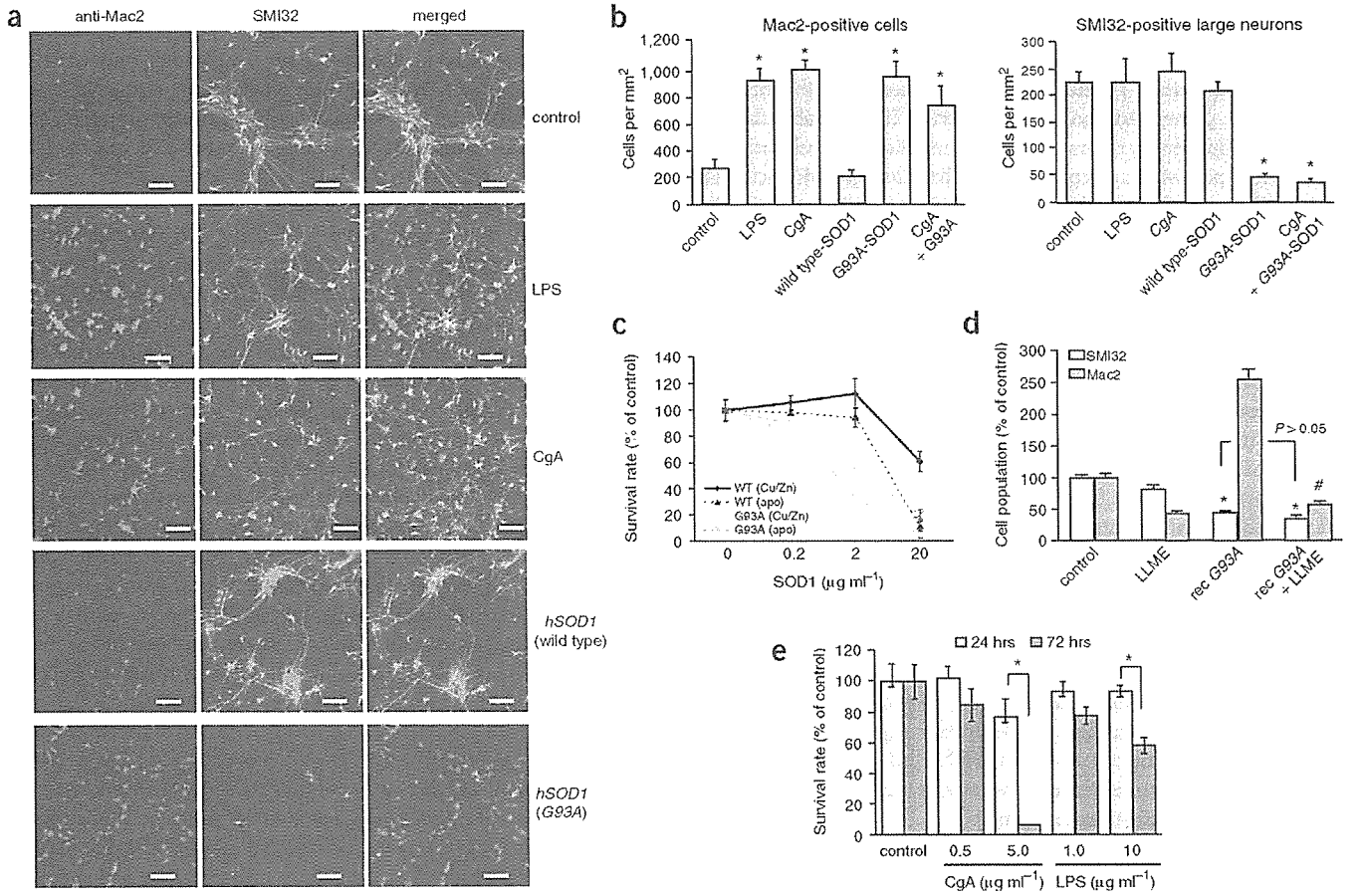

Figure 8 Extracellular SOD1 mutant triggers microgliosis and motor neuron death. **(a)** Immunofluorescence images of primary spinal cultures doubly stained by anti-Mac2 antibody and SMI32. Scale bars, 50 μm. **(b)** Extracellular SOD1 mutant activated microglia and killed motor neurons of embryonic spinal cord cultures. Spinal cord cultures were treated with lipopolysaccharide (LPS, 10 μg ml $^{-1}$), recombinant mouse CgA (5 μg ml $^{-1}$) or recombinant SOD1 (wild-type or G93A, 2 μg ml $^{-1}$) for 24 h. Cultures were fixed with 4% paraformaldehyde and doubly labeled with antibody to Mac2 (top) or antibody to the nonphosphorylated neurofilament NFH (SMI32) (bottom). The number of labeled cells at eight different areas from two sister cultures were averaged and expressed as cells per mm^2. Values indicate mean ± s.e.m. ($n = 8$). *$P < 0.01$ versus controls. **(c)** Dose-dependent toxicity of G93A and wild-type SOD1 in holo- or apo-states to spinal cord cultures. Spinal cultures were exposed to metal-deficient (apo) or metallated (Cu/Zn) recombinant G93A SOD1 or wild-type SOD1 for 24 h. Values indicate mean ± s.e.m. ($n = 8$). **(d)** Elimination of microglia did not affect extracellular SOD1-induced motor neuron death. Cultures were pre-treated with LLME (5 mM) for 16 h before application of recombinant G93A SOD1 (2 μg ml $^{-1}$) for 24 h. Values indicate percent survival compared with control culture (mean ± s.e.m., $n = 8$–24). *$P < 0.01$ versus control, #$P < 0.01$ versus recombinant G93A treatment. **(e)** Motor neuron death caused by longer time exposure to CgA. Spinal cultures were exposed to CgA or LPS for 72 h or 24 h. Values indicate mean ± s.e.m. ($n = 8$). *$P < 0.01$.

G93A SOD1 significantly increased the number of active microglia, like LPS treatment, as determined with antibody specific to Mac2 (**Fig. 8a** and top graph in **Fig. 8b**). On the other hand, whereas exposure to extracellular CgA (5 μg ml $^{-1}$) or LPS (10 μg ml $^{-1}$) for 24 h did not affect the number of motor neurons stained with SMI32 (an antibody that labels unphosphorylated neurofilament-H), recombinant SOD1 mutant (2 μg ml $^{-1}$) caused massive neuronal death (bottom row in **Fig. 8a** and bottom graph in **Fig. 8b**). Thus, both CgA and mutant SOD1 were capable of activating microglia, but only mutant SOD1 was neurotoxic after a 24-h exposure. This toxicity is not related to the metal content, as the apo G93A mutant also exhibited toxicity to motor neurons (**Fig. 8c**). Notably, the apo form of wild-type SOD1 acquired some toxicity at 20 μg ml $^{-1}$ when compared to holo-state wild-type SOD1 (**Fig. 8c**). Furthermore, we investigated the role of microglia in extracellular mutant SOD1–induced motor neuron death by eliminating microglia with exposure to leu-leu methyl ester (LLME), a lysosomotropic agent that kills actively phagocytic cells such as microglia[36]. Treatment of spinal cultures with 5-mM LLME killed approximately 60–70% of Mac2-positive cells; control cultures showed only mild neurotoxicity (**Fig. 8d**). Pretreatment of the cell cultures with LLME did not rescue motor neurons from the toxicity of recombinant SOD1. Although these results indicate that extracellular SOD1 mutant can injure motor neurons independently of microglial activation, the role of microgliosis in motor neuron death cannot be excluded. The viability of motor neurons was affected by extracellular CgA or LPS after longer time exposures (**Fig. 8e**).

DISCUSSION

From the data presented here, we propose a novel pathogenic mechanism for ALS based on chromogranin-mediated secretion of misfolded SOD1 mutants (**Supplementary Fig. 6** online). This model is supported by the following findings: (i) chromogranins interact with ALS-linked SOD1 mutants but not with wild-type SOD1, (ii) chromogranins can promote selective secretion of mutant SOD1, (iii) mutant SOD1 is distributed in the TGN, (iv) extracellular mutant SOD1 can

trigger microgliosis and neuronal death and (v) CgA expression is induced in reactive astrocytes.

It is unclear how the mutant SOD1 proteins are being recruited in the ER-Golgi secretory granule pathway to interact with chromogranins. SOD1 protein has no signal sequence. It is possible that an increased hydrophobicity of mutant SOD1 underlies its translocation in the ER-Golgi pathway, as reported for fibroblast growth factor-16 (ref. 37). The cytosolic soluble protein SOD1 normally maintains its hydrophilicity through intramolecular disulfide bonds. However, mutant SOD1 proteins are readily monomerized by a reducing environment[38], resulting in exposure of hydrophobic regions that can be recognized by Hsp proteins[16]. Once recruited into the ER-Golgi system, it is plausible that oxidative conditions might promote the formation of oligomers, as detected in **Figure 3a**. Our findings are consistent with a previous report that mutant SOD1, but not wild-type SOD1, can induce ER stress when transfected into COS-7 cells, with accumulation of mutant SOD1 in or on the ER[39]. Although we cannot exclude the possibility of a gain of toxic function due to ER stress, our data demonstrate that secretion of mutant SOD1 may represent a toxic pathway which would be in line with the non-cell-autonomous nature of ALS[14].

It is still unclear how mutant SOD1 associates with chromogranins in the ER-Golgi network. The results from our yeast two-hybrid interaction studies support a direct association. Moreover, *in vitro* binding of recombinant CgA with mutant SOD1, but not with wild-type SOD1, was also confirmed (data not shown). The presence of Hsp70-like motifs in both CgB and CgA may explain why chromogranins interact with mutant forms of SOD1, but not with wild-type SOD1. Mutant SOD1 proteins are known to show altered solubility and interact with heat shock/stress proteins[15,16].

Previous studies have shown that wild-type SOD1 can be secreted from cultured astrocytes[40] or thymus-derived cells[41]. Moreover, it has been reported that both wild-type and mutant SOD1 species are detected in the cerebrospinal fluid of both transgenic rats[34] carrying human SOD1 and ALS patients with the SOD1 mutation[35]. Our data together with these observations support the idea that both wild-type and mutant SOD1 proteins may be secreted through non-classical secretory pathways[42]. In addition, we propose a chaperone-like function for chromogranins in mediating the selective secretion of misfolded SOD1 mutants through the ER-Golgi network. In a recent study[35] with NSC34 cells, the secretion was interpreted as being beneficial because the extrusion of mutant SOD1 attenuated formation of toxic intracellular inclusions, ameliorating cell survival. That study did not, however, consider the presence of glial cells in motor neuron environment *in vivo* or the possibility that the disease in not strictly cell autonomous[14]. Conversely, we posit that secretion of mutant SOD1 mediated by chromogranins is deleterious because extracellular mutant SOD1 proteins caused microgliosis and death of embryonic motor neurons in mixed cultures (**Fig. 8**). Unlike secreted mutant SOD1, extracellular wild-type SOD1 probably has protective properties. Our data suggest that extracellular wild-type SOD1 suppresses extracellular inflammation, perhaps through an antioxidant effect (**Fig. 7c**), which would be consistent with the finding that intraspinal infusion of exogenous wild-type SOD1 in G93A SOD1 transgenic rats prolonged their lifespan[34].

From our *in situ* hybridization data and immunohistochemistry of spinal cord samples, it seems that chromogranin expression is elevated in both motor neurons and interneurons (**Supplementary Fig. 2**). Therefore, as depicted in our proposed pathogenic scheme (**Supplementary Fig. 6**), we view interneurons as important contributors to the secretion of chromogranins and mutant SOD1 complexes in the vicinity of motor neurons. In this model, it is the burden of extracellular mutant SOD1 in close proximity to motor neurons that would increase the risk of damage. Even though interneurons and motor neurons themselves would be the predominant source of extracellular mutant SOD1 mediated by chromogranin interactions, mutant SOD1 secreted by other pathways from other cells such as microglia and astrocytes could also contribute to pathogenesis. Though the deleterious effects of intracellular mutant SOD1 can not be excluded, our model of toxicity based on secreted mutant SOD1 is compatible with the idea that the disease is not autonomous to motor neurons[14].

Although the exact mechanisms underlying the microgliosis and neurotoxicity of extracellular mutant SOD1 remain to be elucidated, various deleterious effects of misfolded SOD1 proteins may occur through generation of hydroxyl radicals[7], toxic oligomers[11] or amyloid-like filaments[43]. This model would support a linkage between inflammation and ALS pathogenesis[44,45]. Many factors may contribute to motor neuron death in the context of inflammation. Proinflammatory molecules such as TNF-α, Fas ligand or nitric oxide may act as mediators of motor neuron death[8]. Microglial activation alone is not usually sufficient to induce motor neuron death. For instance, induction of innate immunity by intraperitoneal injection of LPS does not injure motor neurons[44]. Chronic LPS administration precipitated ALS in mice, however, supporting the view that chronic inflammation may constitute a risk factor[44]. Yet, our data demonstrate that elimination of microglia by LLME did not alter survival of motor neurons and that LPS is much less toxic to motor neurons than mutant SOD1 in mixed embryonic spinal cord cultures (**Fig. 8b,e**). It is noteworthy that mutant SOD1, and to some extent wild-type SOD1, can be converted to toxic species even in absence of copper and zinc (**Fig. 8c**). This concurs with previous reports about the misfolded nature of apo-state SOD1 (refs. 16,43).

In conclusion, our results suggest a novel function for chromogranins in mediating the secretion of misfolded SOD1 mutants, a potentially toxic pathway that can induce inflammation and neuronal death. In future studies, it will be of interest to determine whether chromogranin-mediated secretion may be applicable to other neurodegenerative diseases that involve misfolded proteins.

METHODS

Materials. Commercially available antibodies are listed in **Supplementary Methods** online. The Golgi marker plasmid DsRed-Golgi, which carries the Golgi-targeting sequence of the human gene encoding β1,4-galactosyl transferase, was a generous gift from Y. Imai (RIKEN Brain Science Institute).

To generate an antibody specific to the N′ terminus of mouse CgA, we immunized rabbits with the peptide CLPVNSPMTKGDTKVMK, which encodes the amino terminal residues of mature mouse CgA (amino acids 18–35). The antisera were purified with an affinity column coupled with the same antigen. The titer and specificity were investigated by western blotting (**Supplementary Fig. 4**).

The recombinant proteins of human SOD1 (wild-type and mutant) and mouse CgA were generated from *Escherichia coli* as described in **Supplementary Methods**.

Transgenic mice. Transgenic mice harboring the G93A mutant of human *SOD1* (*B6SJL-TgN[SOD1-G93A]^{dl}1Gur*, *B6SJL-TgN[SOD1-G93A]1Gur*) and those harboring wild-type human *SOD1* (*C57Bl/6-TgN[SOD1]3Cje*, *hSOD1^{WT}*) were purchased from The Jackson Laboratory. Transgenic mice carrying G37R *SOD1* (line 29) were a kind gift from D. Cleveland (University of California, San Diego) and were housed and bred with C57Bl/6 mice. We selected these mouse lines because they were readily available to us. Since we maintain a larger colony of G37R *SOD1* (line 29) mice, most of our experiments involving mouse analysis were done with this line. Mice were treated with 10% chloral hydrate for anesthesia before they were perfused or killed. Animals were handled in accordance with the approved protocol by the animal experiment committees at RIKEN Brain Science Institute and by the Comité de Protection des Animaux de l'Université Laval.

Yeast two-hybrid screening. The plasmid *pGilda* carrying the G93A *SOD1* mutant was generated as bait for library screening. Yeast two-hybrid analysis (LexA/transactivation system) was performed on a cDNA library (1.5 10^6 independent clones) ligated into the *pJG4,5* plasmid from the total spinal cords of five preclinical transgenic mice carrying human G93A *SOD1* (*B6SJL-Tg(SOD1-G93A)1Gur/J*). Yeast two-hybrid screening was carried out using the Matchmaker Two-Hybrid System (Clontech) according to the manufacturer's protocol. There were 250 blue colonies that survived on the agar plates that contained galactose/raffinose and X-gal, but lacked tryptophan, histidine, leucine and uracil. All 250 were sequenced.

Plasmids, cell culture and transfection. Expression plasmids harboring human *SOD1* (wild-type, A4V, G85R or G93A) were prepared as reported previously[11]. The full-length murine genes encoding CgA (*Chga*) or CgB (*Chgb*) were cloned by RT-PCR using polyA-RNA from total brain of adult normal mice of the C57Bl/6 strain. See **Supplementary Methods** and **Supplementary Table 1** online for construction of EGFP-tagged CgB or deletion mutants of CgB. Cells from the murine neuroblastoma cell line Neuro2a, from the mouse fibroblast cell line NIH3T3 and COS-7 monkey ovary cells were maintained in nutrient medium containing 10% fetal bovine serum in the Dulbecco's minimal essential medium (DMEM, Sigma). The mouse microglial BV2 cells were cultured in DMEM-F12 Ham's (DF) medium containing 10% FBS. Cells were used for transfection using Lipofectamine Plus (Invitrogen) according to the manufacturer's protocol.

Immunoblotting and immunoprecipitation of cultured cells. Cells were lysed in TNT-G buffer consisting of 50 mM Tris-HCl (pH 7.4), 150 mM NaCl and 1% Triton-X100 with protease inhibitor cocktail (Roche) 24 h after the transfection. The cell lysates were incubated with anti-FLAG M2 agarose affinity gel (Sigma) for 1 h at 4 °C and were eluted with 4% SDS sample buffer. Samples were resolved by SDS-PAGE and transferred to a PVDF membrane (Polyscreen, PerkinElmer). A western blot image was obtained using a chemiluminescence detection kit (PerkinElmer).

Immunofluorescence and immunohistochemistry. Fixation of the cells and preparation of spinal cord slices is described in **Supplementary Methods.** After blocking, cultures or sections were incubated with primary antibodies and subsequently with corresponding fluorescent secondary antibodies (Alexa, Invitrogen) or with biotinylated secondary antibodies visualized by the avidin-biotin-immunoperoxidase complex (ABC) method using a Vectastain ABC kit (Vector Laboratories) and 3.3′-diaminobenzidine tetrahydrochloride (DAB; Sigma). The dilution rate of the primary antibodies is indicated in **Supplementary Methods.** Cells and tissue sections were observed by confocal laser microscopy (Olympus).

Subcellular fractionation of the spinal cord lysates. Spinal cord tissues from different ages of human *SOD1* transgenic mice were subcellularly fractionated into cytosolic, heavy and light membrane fractions, as described in **Supplementary Methods.** The protein concentration was determined by Bradford assay (BioRad), and an equal amount of protein was analyzed by western blotting. The percentage distribution of hSOD1 in post-nuclear fractions was also obtained by densitometric analysis and calculation of proportion from initial volume.

Sucrose-gradient ultracentrifugation of microsome fraction from spinal cord lysates. The light membrane (microsomal) fraction from spinal cord of *G37R SOD1* mice was further separated by sucrose gradient ultracentrifugation as previously described[46], with minor modifications that are decribed in **Supplementary Methods.** After overnight ultracentrifugation in sucrose cushions (5%, 30% and 40%), one-tenth (0.42 ml) was taken from the top of each sample, and the pellet was resuspended in MBS with 2 mM EDTA and 1% Triton-X100, and then concentrated using a centrifugal filter (Millipore) to 100 µl. Each fraction (20 µl) was separated by SDS-PAGE and analyzed by western blotting.

Immuno-isolation of TGN. To obtain pure preparations of TGN, we generated rabbit polyclonal antibody specific to the amino terminal peptides (CEGKRSKVTRRPKASDYQRLNLKL) of mouse/rat TGN38, a surface marker of TGN[47]. This anti-TGN38 or rabbit control IgG was bound to protein G-coated magnetic beads (Dynal) and was incubated with precleared post-mitochondrial fractions (described in more detail in **Supplementary Methods**). After washing, immunoprecipitates were eluted by 4% SDS sampling buffer and analyzed by western blotting with human SOD1-specific antibody (StressGen).

Immunoprecipitation of spinal cord lysates. The post-mitochondrial fractions of spinal cords were prepared by the same protocol as those in the immuno-isolation experiments. Rabbit polyclonal antibodies to CgA or CgB (Santa Cruz) or rabbit control IgG was bound to protein G-coated magnetic beads and incubated with precleared lysates, as described in **Supplementary Methods.** Immunoprecipitates were analyzed by Western blotting with human SOD1-specific antibody (StressGen).

Immunoelectron microscopy. We used post-embedding immunohistochemistry for electron microscopic observation, in which ultra-thin sections on the nickel grids were processed for immunohistochemistry without osmication. Fixation of the mice and preparation of ultrathin sections are described in **Supplementary Methods.** After blocking, grids were incubated with primary antibodies in the same buffer at 4 °C overnight, followed by a reaction with immunogold-conjugated secondary antibody (10 nm or 5 nm) for 1 h at 22 °C. For double staining, grids were further processed using another immunoreaction with a different primary and the secondary antibody with differently sized gold particles. Grids were observed by a TECNAI 12 electron microscope (FEI company).

Secretion assays. COS-7 and NIH3T3 cells were used in secretion experiments as non-neuronal cells lacking secretory granules[33]. At 24 h after transfection, cells plated onto a 6-well culture dish were washed in prewarmed PBS twice. Cells were incubated in basal secretion medium containing 10 mM HEPES, 129 mM NaCl, 5 mM $NaHCO_3$, 4.8 mM KCl, 1.2 mM $MgCl_2$, 1.2 mM KH_2PO_4, 1 mM $CaCl_2$ and 2.8 mM glucose (pH 7.4) for 1 h, and then treated with 1 ml of secretagogue-containing medium (stimulation buffer: 10 mM Hepes, 79 mM NaCl, 5 mM $NaHCO_3$, 50 mM KCl, 1.2 mM KH_2PO_4, 1.2 mM $MgCl_2$, 2 mM $BaCl_2$, 2.8 mM glucose, pH 7.4) for 15 min. In some experiments, Brefeldin A (BFA, 5 µM) was applied before exposure to stimulation medium. Lactacystin was applied in some assays 3 h after transfection and before incubation with basal buffer. We then collected 950 µl of medium and centrifuged it for 5 min at 1,000*g* to remove the debris. The supernatants were concentrated by a protein concentrator with 3.5 kDa cut-off (Millipore) to 60 µl, followed by western analysis. Secreted SOD1 was estimated by standardization with intracellular SOD1 in total cell lysates.

Primary cultures from embryonic spinal cord of transgenic mice carrying human *SOD1* (wild-type or *G37R*) were also investigated by secretion analysis. Cultures were prepared as explained below. Cell suspension from one spinal cord was plated onto one chamber in a six-well culture plate coated with polyethyleneimine. Secretion experiments were done after 14 d of culture *in vitro* using the protocol described above.

The content of LDH in the culture medium was measured in the medium 24 h after transfection using an LDH assay kit (Promega) according to the manufacture's protocol. Cells transfected with empty vector were used as a control.

Semi-quantitative reverse transcription PCR of microglial cell lines. Neuro2a cells were co-transfected with *pcDNA-SOD1* (wild-type, *G85R* or *G93A*) and *pcDNA3-CgA* in DF medium containing 10% FBS. At 16 h after transfection, the conditioned medium was transferred into the culture wells where BV2 cells had been previously plated, then further incubated for 24 h. Alternatively, BV2 cells were treated directly with recombinant proteins for 24 h. Then, cells were washed twice in PBS and total RNA was extracted using Trizol (Invitrogen). RT-PCR was conducted using oligo-dT primers according to the manufacturer's protocol (Invitrogen). The sequence of primer pairs is shown in **Supplementary Table 2** online. The gel images of PCR products obtained from illuminator were scanned, and densitometric analysis was performed using Scion image (Scion Corp.).

Primary culture of mouse embryonic spinal cord. Dissociated cultures of embryonic murine spinal cord were grown as previously described[11]. The spinal

cultures were treated at 11 or 14 d after plating. Motor neurons were identified as large cells labeled with SMI32 and active microglia were detected with Mac2-specific antibody. Confocal microscopy images were obtained from eight randomly selected fields, and immunoreactive cells were counted by computer. In several experiments, microglia were eliminated by a 16-h treatment with LLME[36] before exposure to recombinant SOD1 proteins. In preliminary experiments, we noticed that 5-mM LLME for 16 h killed approximately 60–70% of Mac2-positive cells. The number of cells was calculated as cells per mm^2 and averaged. Statistical significance was evaluated by single-factor ANOVA (analysis of variance) following Scheffe's method.

Note: Supplementary information is available on the Nature Neuroscience website.

ACKNOWLEDGMENTS

We thank R. Janvier for sample preparation for immunoelectron microscopy and B. Gentil for advice on experimental procedures. The technical help from G. Soucy, S.A. Ezzi (Laval University) and J. Kurisu (RIKEN Brain Science Institute) is appreciated. We thank D. Cleveland (University of California San Diego) for the G37R *SOD1* transgenic mice and Y. Imai for the *DsRed-Golgi* plasmid. This work was supported by the Canadian Institutes of Health Research (CIHR), the Robert Packard Centre for ALS Research at Johns Hopkins, the ALS Association (USA), the ALS Society of Canada, the Japan Society for the Promotion of Science (JSPS) and the Japan Foundation for Neuroscience and Mental Health. J.-P.J. holds a Canada Research Chair in Neurodegeneration. M.U. is a recipient of a Uehara Memorial Foundation research fellowship and a postdoctoral fellowship from CIHR.

COMPETING INTERESTS STATEMENT

The authors declare that they have no competing financial interests.

Published online at http://www.nature.com/natureneuroscience/
Reprints and permissions information is available online at http://npg.nature.com/reprintsandpermissions/

1. Rosen, D.R. *et al.* Mutations in Cu/Zn superoxide dismutase gene are associated with familial amyotrophic lateral sclerosis. *Nature* **362**, 59–62 (1993).
2. Gurney, M.E. *et al.* Motor neuron degeneration in mice that express a human Cu,Zn superoxide dismutase mutation. *Science* **264**, 1772–1775 (1994).
3. Subramaniam, J.R. *et al.* Mutant SOD1 causes motor neuron disease independent of copper chaperone-mediated copper loading. *Nat. Neurosci.* **5**, 301–307 (2002).
4. Wang, J., Xu, G. & Borchelt, D.R. High molecular weight complexes of mutant superoxide dismutase 1: age-dependent and tissue-specific accumulation. *Neurobiol. Dis.* **9**, 139–148 (2002).
5. Julien, J.P. Amyotrophic lateral sclerosis. unfolding the toxicity of the misfolded. *Cell* **104**, 581–591 (2001).
6. Cleveland, D.W. & Rothstein, J.D. From Charcot to Lou Gehrig: deciphering selective motor neuron death in ALS. *Nat. Rev. Neurosci.* **2**, 806–819 (2001).
7. Wiedau-Pazos, M. *et al.* Altered reactivity of superoxide dismutase in familial amyotrophic lateral sclerosis. *Science* **271**, 515–518 (1996).
8. Raoul, C. *et al.* Motoneuron death triggered by a specific pathway downstream of Fas: potentiation by ALS-linked SOD1 mutations. *Neuron* **35**, 1067–1083 (2002).
9. Durham, H.D., Roy, J., Dong, L. & Figlewicz, D.A. Aggregation of mutant Cu/Zn superoxide dismutase proteins in a culture model of ALS. *J. Neuropathol. Exp. Neurol.* **56**, 523–530 (1997).
10. Johnston, J.A., Dalton, M.J., Gurney, M.E. & Kopito, R.R. Formation of high molecular weight complexes of mutant Cu, Zn-superoxide dismutase in a mouse model for familial amyotrophic lateral sclerosis. *Proc. Natl. Acad. Sci. USA* **97**, 12571–12576 (2000).
11. Urushitani, M., Kurisu, J., Tsukita, K. & Takahashi, R. Proteasomal inhibition by misfolded mutant superoxide dismutase 1 induces selective motor neuron death in familial amyotrophic lateral sclerosis. *J. Neurochem.* **83**, 1030–1042 (2002).
12. Pramatarova, A., Laganière, J., Roussel, J., Brisebois, K. & Rouleau, G.A. Neuron-specific expression of mutant superoxide dismutase 1 in transgenic mice does not lead to motor impairment. *J. Neurosci.* **21**, 3369–3374 (2001).
13. Lino, M.M., Schneider, C. & Caroni, P. Accumulation of SOD1 mutants in postnatal motoneurons does not cause motoneuron pathology or motoneuron disease. *J. Neurosci.* **22**, 4825–4832 (2002).
14. Clement, A.M. *et al.* Wild-type nonneuronal cells extend survival of SOD1 mutant motor neurons in ALS mice. *Science* **302**, 113–117 (2003).
15. Shinder, G.A., Lacourse, M.C., Minotti, S. & Durham, H.D. Mutant Cu/Zn-superoxide dismutase proteins have altered solubility and interact with heat shock/stress proteins in models of amyotrophic lateral sclerosis. *J. Biol. Chem.* **276**, 12791–12796 (2001).
16. Urushitani, M. *et al.* CHIP promotes proteasomal degradation of familial ALS-linked mutant SOD1 by ubiquitinating Hsp/Hsc70. *J. Neurochem.* **90**, 231–244 (2004).
17. Taupenot, L., Harper, K.L. & O'Connor, D.T. The chromogranin-secretogranin family. *N. Engl. J. Med.* **348**, 1134–1149 (2003).
18. Rudolf, R., Salm, T., Rustom, A. & Gerdes, H.H. Dynamics of immature secretory granules: role of cytoskeletal elements during transport, cortical restriction, and f-actin-dependent tethering. *Mol. Biol. Cell* **12**, 1353–1365 (2001).
19. Li, J.Y., Leitner, B., Lovisetti-Scamihorn, P., Winkler, H. & Dahlström, A. Proteolytic processing, axonal transport and differential distribution of chromogranins A and B, and secretogranin II (secretoneurin) in rat sciatic nerve and spinal cord. *Eur. J. Neurosci.* **11**, 528–544 (1999).
20. Booj, S., Goldstein, M., Fischer-Colbrie, R. & Dahlstrom, A. Calcitonin gene-related peptide and chromogranin A: presence and intra-axonal transport in lumbar motor neurons in the rat, a comparison with synaptic vesicle antigens in immunohistochemical studies. *Neuroscience* **30**, 479–501 (1989).
21. Marksteiner, J. *et al.* Distribution of chromogranin B-like immunoreactivity in the human hippocampus and its changes in Alzheimer's disease. *Acta Neuropathol. (Berl.)* **100**, 205–212 (2000).
22. Rangon, C.M. *et al.* Different chromogranin immunoreactivity between prion and a-beta amyloid plaque. *Neuroreport* **14**, 755–758 (2003).
23. Schiffer, D., Cordera, S., Giordana, M.T., Attanasio, A. & Pezzulo, T. Synaptic vesicle proteins, synaptophysin and chromogranin A in amyotrophic lateral sclerosis. *J. Neurol. Sci.* **129** Suppl, 68–74 (1995).
24. Taupenot, L. *et al.* Chromogranin A triggers a phenotypic transformation and the generation of nitric oxide in brain microglial cells. *Neuroscience* **72**, 377–389 (1996).
25. Ciesielski-Treska, J. *et al.* Mechanisms underlying neuronal death induced by chromogranin A-activated microglia. *J. Biol. Chem.* **276**, 13113–13120 (2001).
26. Taylor, D.L., Diemel, L.T. & Pocock, J.M. Activation of microglial group III metabotropic glutamate receptors protects neurons against microglial neurotoxicity. *J. Neurosci.* **23**, 2150–2160 (2003).
27. Chanat, E., Weiss, U., Huttner, W.B. & Tooze, S.A. Reduction of the disulfide bond of chromogranin B (secretogranin I) in the trans-Golgi network causes its missorting to the constitutive secretory pathways. *EMBO J.* **12**, 2159–2168 (1993).
28. Cowley, D.J., Moore, Y.R., Darling, D.S., Joyce, P.B. & Gorr, S.U. N- and C-terminal domains direct cell type-specific sorting of chromogranin A to secretory granules. *J. Biol. Chem.* **275**, 7743–7748 (2000).
29. Li, J.Y., Kling-Petersen, A. & Dahlstrom, A. Influence of spinal cord transection on the presence and axonal transport of CGRP-, chromogranin A-, VIP-, synapsin I-, and synaptophysin-like immunoreactivities in rat motor nerve. *J. Neurobiol.* **23**, 1094–1110 (1992).
30. Kato, A. *et al.* Co-distribution patterns of chromogranin B-like immunoreactivity with chromogranin A and secretoneurin within the human brainstem. *Brain Res.* **852**, 444–452 (2000).
31. Stieber, A. *et al.* Disruption of the structure of the Golgi apparatus and the function of the secretory pathway by mutants G93A and G85R of Cu, Zn superoxide dismutase (SOD1) of familial amyotrophic lateral sclerosis. *J. Neurol. Sci.* **219**, 45–53 (2004).
32. Ciesielski-Treska, J. *et al.* Chromogranin A induces a neurotoxic phenotype in brain microglial cells. *J. Biol. Chem.* **273**, 14339–14346 (1998).
33. Huh, Y.H., Jeon, S.H. & Yoo, S.H. Chromogranin B-induced secretory granule biogenesis: comparison with the similar role of chromogranin A. *J. Biol. Chem.* **278**, 40581–40589 (2003).
34. Turner, B.J. *et al.* Impaired extracellular secretion of mutant superoxide dismutase 1 associates with neurotoxicity in familial amyotrophic lateral sclerosis. *J. Neurosci.* **25**, 108–117 (2005).
35. Jacobsson, J., Jonsson, P.A., Andersen, P.M., Forsgren, L. & Marklund, S.L. Superoxide dismutase in CSF from amyotrophic lateral sclerosis patients with and without CuZn-superoxide dismutase mutations. *Brain* **124**, 1461–1466 (2001).
36. Sharpless, N. *et al.* The restricted nature of HIV-1 tropism for cultured neural cells. *Virology* **191**, 813–825 (1992).
37. Miyakawa, K. & Imamura, T. Secretion of FGF-16 requires an uncleaved bipartite signal sequence. *J. Biol. Chem.* **278**, 35718–35724 (2003).
38. Tiwari, A. & Hayward, L.J. Familial amyotrophic lateral sclerosis mutants of copper/zinc superoxide dismutase are susceptible to disulfide reduction. *J. Biol. Chem.* **278**, 5984–5992 (2003).
39. Tobisawa, S. *et al.* Mutant SOD1 linked to familial amyotrophic lateral sclerosis, but not wild-type SOD1, induces ER stress in COS7 cells and transgenic mice. *Biochem. Biophys. Res. Commun.* **303**, 496–503 (2003).
40. Lafon-Cazal, M. *et al.* Proteomic analysis of astrocytic secretion in the mouse. Comparison with the cerebrospinal fluid proteome. *J. Biol. Chem.* **278**, 24438–24448 (2003).
41. Cimini, V. *et al.* CuZn-superoxide dismutase in human thymus: immunocytochemical localisation and secretion in thymus-derived epithelial and fibroblast cell lines. *Histochem. Cell Biol.* **118**, 163–169 (2002).
42. Nickel, W. The mystery of nonclassical protein secretion. A current view on cargo proteins and potential export routes. *Eur. J. Biochem.* **270**, 2109–2119 (2003).
43. Elam, J.S. *et al.* Amyloid-like filaments and water-filled nanotubes formed by SOD1 mutant proteins linked to familial ALS. *Nat. Struct. Biol.* **10**, 461–467 (2003).
44. Nguyen, M.D., D'Aigle, T., Gowing, G., Julien, J.P. & Rivest, S. Exacerbation of motor neuron disease by chronic stimulation of innate immunity in a mouse model of amyotrophic lateral sclerosis. *J. Neurosci.* **24**, 1340–1349 (2004).
45. Zhu, S. *et al.* Minocycline inhibits cytochrome c release and delays progression of amyotrophic lateral sclerosis in mice. *Nature* **417**, 74–78 (2002).
46. Parkin, E.T., Hussain, I., Karran, E.H., Turner, A.J. & Hooper, N.M. Characterization of detergent-insoluble complexes containing the familial Alzheimer's disease-associated presenilins. *J. Neurochem.* **72**, 1534–1543 (1999).
47. Stephens, D.J. & Banting, G. Direct interaction of the trans-Golgi network membrane protein, TGN38, with the F-actin binding protein, neurabin. *J. Biol. Chem.* **274**, 30080–30086 (1999).

The neuropeptide head activator is a high-affinity ligand for the orphan G-protein-coupled receptor GPR37

Meriem Rezgaoui[1], Ute Süsens[1], Atanas Ignatov[1], Mathias Gelderblom[2], Günter Glassmeier[3], Inga Franke[1], Jens Urny[1], Yuzuru Imai[4], Ryosuke Takahashi[4] and H. Chica Schaller[1,*]

[1]Zentrum für Molekulare Neurobiologie Hamburg, [2]Klinik und Poliklinik für Neurologie, and [3]Institut für Angewandte Physiologie, Universitätsklinikum Hamburg-Eppendorf, Martinistr. 52, 20246 Hamburg, Germany
[4]RIKEN Brain Science Institute, Saitama 351-0198, Japan
*Author for correspondence (e-mail: schaller@zmnh.uni-hamburg.de)

Accepted 26 October 2005
Journal of Cell Science 119, 542-549 Published by The Company of Biologists 2006
doi:10.1242/jcs.02766

Summary

The neuropeptide head activator (HA) is a mitogen for mammalian cell lines of neuronal or neuroendocrine origin. HA signalling is mediated by a G-protein-coupled receptor (GPCR). Orphan GPCRs with homology to peptide receptors were screened for HA interaction. Electrophysiological recordings in frog oocytes and in mammalian cell lines as well as Ca^{2+} mobilisation assays revealed nanomolar affinities of HA to GPR37. HA signal transduction through GPR37 was mediated by an inhibitory G protein and required Ca^{2+} influx through a channel of the transient receptor potential (TRP) family. It also required activation of Ca^{2+}-dependent calmodulin kinase and phosphoinositide 3-kinase. Respective inhibitors blocked HA signalling and HA-induced mitosis in GPR37-expressing cells. HA treatment resulted in internalisation of GPR37. Overexpression of GPR37 led to aggregate formation, retention of the receptor in the cytoplasm and low survival rates of transfected cells, confirming the notion that misfolded GPR37 contributes to cell death, as observed in Parkinson's disease.

Key words: G-protein-coupled receptor, GPR37, Head activator, Pael receptor, Parkinson, Signal transduction

Introduction

The undecapeptide head activator (HA) was originally isolated and characterised from hydra, where it mediates head-specific growth and differentiation processes, hence its name. In hydra, HA is produced by nerve cells and is stored in neurosecretory granules, from which it is released to initiate head regeneration and budding, and to maintain the normal head-to-foot morphology of hydra. At the cellular level, HA promotes proliferation of all cell types of hydra by acting as mitogen in the G2-mitosis transition; as for early mammalian development, this transition is the most important checkpoint to control cell-cycle progression. At higher concentrations, HA acts on the determination of stem cells to head-specific fates (Schaller et al., 1996).

HA was isolated with identical sequence from mammalian brain and intestine (Bodenmuller and Schaller, 1981). In adult mammals, HA enhances neurite outgrowth and is neuroprotective. HA is present during early mammalian development and is expressed in cells of the nervous and neuroendocrine system. Like in hydra, HA stimulates entry into mitosis and proliferation of cell lines derived from such origins. The signalling cascade from HA to mitosis includes activation of an inhibitory G protein and requires Ca^{2+} influx, downregulation of adenylyl cyclase and hyperpolarisation of the membrane potential (Kayser et al., 1998; Niemann and Schaller, 1996; Ulrich et al., 1996). For Ca^{2+} influx, a transient receptor potential (TRP)-like channel is responsible, which can be regulated by growth factors, such as insulin growth factor I (IGF-I) and platelet-derived growth factor (PDGF) (Kanzaki et al., 1999), and by HA (Boels et al., 2001). The increase in intracellular Ca^{2+} then triggers influx of K^+ through a Ca^{2+}-activated K^+ channel, leading to hyperpolarisation, which is an absolute requirement for entry into mitosis (Kayser et al., 1998).

In the search for receptors mediating the action of HA on stimulating mitosis in mammalian cells, we concentrated on orphan G-protein-coupled receptors (GPCRs) reacting with small peptides as ligands. GPCRs are the largest family of cell-surface receptors that mediate transduction of signals from the extracellular environment to intracellular effectors. They contain seven transmembrane domains and are activated by ligands of extremely different molecular origins and sizes including light, ions, metabolic intermediates, amino acids, nucleotides, lipids, peptides and proteins. These ligands primarily interact with the extracellular domains, but in part also with transmembrane regions of GPCRs. The classification of GPCRs into subfamilies is primarily based on their homology within the heptahelical structure (Frederiksson et al., 2003), but also on extracellular domains, and has been used to predict ligands for orphan receptors (Boels and Schaller, 2003; Ignatov et al., 2003a; Ignatov et al., 2003b). To find a receptor for HA, we concentrated on GPCR subfamilies reacting with small peptides as ligands.

Several orphan receptors failed to show interactions with HA, including GPR6 and GPR12, for which we found lysophospholipids as cognate ligands (Ignatov et al., 2003a;

Journal of Cell Science

Ignatov et al., 2003b). HA had no effect on GPR99, GPR100, GalRL, GPR1, GPR7, GPR8, GPR19, GPR75 and SALPR, just to name a few. Of special interest was a sub-branch of GPCRs that regulate cellular proliferation, namely the endothelin, bombesin and neuromedin receptors. Two orphan receptors are part of this group: GPR37 and GPR37L1 (Marazziti et al., 2001). We focused our interest on GPR37 because of its prominent expression in neurons of the brain compared with a more glial location of GPR37L1 (Marazziti et al., 1997; Zeng et al., 1997). GPR37 has also been isolated and characterised as a substrate for the ubiquitin ligase parkin, hence its alternative name – parkin-associated endothelin-like receptor (Pael R) (Imai et al., 2001). GPR37 was shown to fold improperly in the absence of parkin, and its aggregation to insoluble complexes results in endoplasmic reticulum stress (Imai et al., 2001; Imai et al., 2003). This leads to preferential loss of dopaminergic neurons in the substantia nigra and contributes to neurodegeneration in Parkinson's disease (Yang et al., 2003). Accumulation of GPR37 in Lewy bodies in the brain of patients with Parkinson's disease supports this notion (Murakami et al., 2004).

To study a possible interaction of HA with GPR37, various assay systems were used that allow detection, directly or indirectly, of ligand-receptor interactions. In this paper, we present evidence that HA is a high-affinity ligand for GPR37.

Results

HA stimulates internalisation of GPR37 in COS-7 cells

We tried to express GPR37 heterologously in Chinese hamster ovary (CHO-K1) cells, in human embryonic kidney (HEK-293) cells and in green monkey kidney (COS-7) cells. Transient transfection efficiencies in HEK-293 and CHO-K1 cells were far below 5%, and cells expressing GPR37 looked sick and decreased in number at 48 hours compared with 24 hours after transfection. Transfection efficiencies in COS-7 cells were better and reached levels in the range of 15-30% (Fig. 1A). COS-7 cells were therefore suitable for experiments with individual, transfected cells. There was no difference in expression levels between GPR37 with (Fig. 1B) and without (Fig. 1C) FLAG tag at the C-terminus. This indicated that the tag did not interfere with GPR37 protein biosynthesis and localisation. GPR37 immunoreactivity was visible in the cytoplasm of transfected COS-7 cells, but also extended to cell protrusions, hinting at cell-surface expression (Fig. 1B,C). Cell-surface expression was confirmed by treating living cells before fixation with a monoclonal antibody against GPR37 (Fig. 1D) that reacts with extracellular epitopes of GPR37 (Imai et al., 2001).

HA treatment of COS-7 cells transiently transfected with GPR37-FLAG led to internalisation of the receptor. This was visible as disappearance of the GPR37-FLAG immunoreactivity from the protrusions after 10 minutes (compare Fig. 1E and F), and as translocation into the cytoplasm after 20 minutes (Fig. 1G). Protrusions started to show FLAG staining again after 30-60 minutes (Fig. 1H,I).

GPR37 aggregation is prevented by stable inducible expression in HEK-293 cells

Transient expression of GPR37 led in all cell lines assayed to aggregation of complexes with apparent molecular masses of 250 kDa (Fig. 2A). Surface biotinylation showed that only the monomeric receptor appeared at the outer cell membrane (Fig. 2B), indicating that most of the overproduced GPR37 was not properly folded, stayed in the cytoplasm and was probably

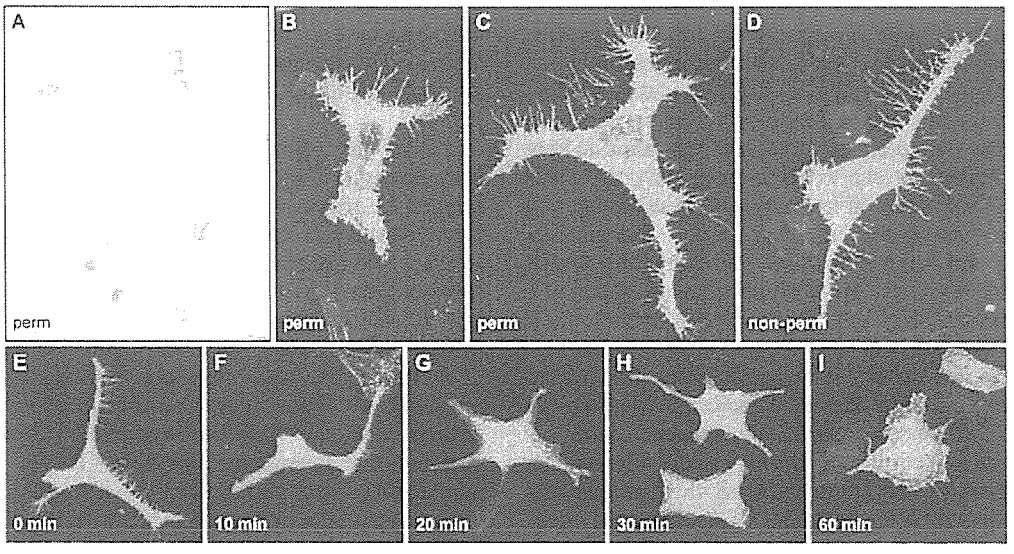

Fig. 1. GPR37 is expressed at the cell surface of COS-7 cells and internalises after HA treatment. (A-I) COS-7 cells were transfected with GPR37 with (B,D-I) or without (A,C) FLAG tag, immunostained with anti-GPR37 antibody (A,C,D) or with anti-FLAG antibody (B,E-I) and visualised with alkaline phosphatase-coupled secondary antibodies for light microscopy (A) or with Cy3-coupled antibodies for confocal analysis (B-I). Cells were permeabilised (perm) by fixation with 1% acetic acid in ethanol and by washing with Triton X-100, except in D, where living cells were incubated with the primary antibody before fixation (non-perm) to show surface staining. (E-I) COS-7 cells 48 hours after transfection with GPR37-FLAG were treated at 37°C with 2 nM HA for 0, 10, 20, 30 and 60 minutes, respectively, and immunostained with anti-FLAG antibody.

degraded (Imai et al., 2001). To prevent aggregation and subsequent degradation, we integrated GPR37 stably into HEK-T-REx cells with a construct that allowed induction by tetracycline (HEK-T-REx–GPR37). Incubation of cells with the tetracycline derivative doxycycline for 24 hours resulted in production predominantly of the monomeric form of GPR37 (Fig. 2C, first lane). Without doxycycline induction, GPR37 was not detectable (Fig. 2C, second lane). Confocal image analysis revealed that, after induction with doxycycline, GPR37 localised mainly to the outer cell membrane, both in permeabilised (Fig. 2D) and non-permeabilised cells (Fig. 2F). The non-induced cells showed no GPR37 immunoreactivity (Fig. 2E,G). To study internalisation, HEK-T-REx–GPR37 cells were incubated in defined medium for 24 hours with doxycycline to induce GPR37 expression. Subsequent treatment with HA for 10 minutes led to rapid internalisation of GPR37 (Fig. 2H,I). This internalisation was much faster in HEK than in COS-7 cells, probably as a result of differences in -arrestin levels (Ménard et al., 1997).

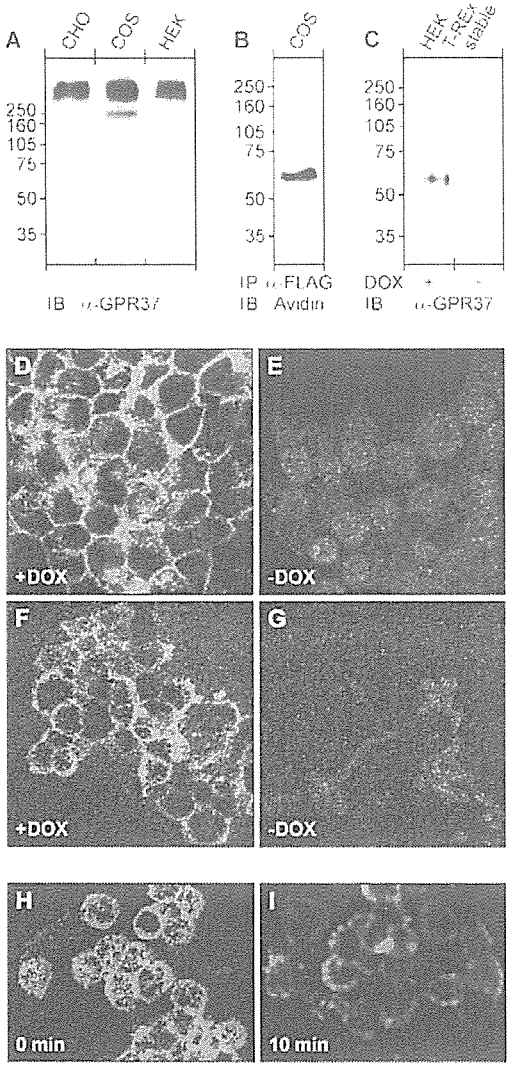

Fig. 2. Inducible, stable expression of GPR37 prevents aggregate formation. (A) CHO-K1, COS-7 and HEK-293 cells were transiently transfected with GPR37, and membrane fractions were assayed by immunoblotting (IB) with anti-GPR37 antibody (-GPR37). (B) COS-7 cells transiently transfected with GPR37-FLAG were cell-surface biotinylated, and the solubilised membrane fraction was immunoprecipated (IP) with anti-FLAG antibody (-FLAG) and visualised after immunoblotting with avidin. (C) GPR37 was introduced stably into the flip-in cell line HEK-T-REx, where GPR37 expression is inducible by doxycycline (DOX). Membrane fractions were subjected to western blotting with anti-GPR37 antibody (-GPR37) with (first lane) and without (second lane) induction for 24 hours with doxycycline. (D-I) HEK-T-REx–GPR37 cells with (D,F,H,I) and without (E,G) doxycycline induction for 24 hours were immunostained with anti-GPR37(R2) antibody after permeabilisation (D,E) and with anti-GPR37 antibody without permeabilisation (F-I). (H,I) HEK-T-REx–GPR37 cells were treated with 2 nM HA for 0 and 10 minutes at 37°C, respectively, fixed with 2% formaldehyde for 10 minutes and subsequently immunostained with anti-GPR37 antibody.

HA binds to GPR37

To show direct interaction of HA with GPR37, COS-7 cells were analysed after incubation with 2 nM HA by fluorescence resonance energy transfer (FRET). Localisation of HA was detected with a HA-specific polyclonal antiserum and was visualised with a Cy2-coupled secondary antibody (green). To detect GPR37, monoclonal antibodies directed against the extracellular domain of human GPR37 were used in combination with a Cy3-coupled secondary antibody (red). Fig. 3A-D shows a typical example of FRET between HA and ectodomains of GPR37. After bleaching a discrete area in a GPR37-positive cell (Fig. 3A,B), an increase in HA fluorescence was observed (Fig. 3C,D). The difference in staining pattern is due to the fact that COS-7 cells, in addition to GPR37, express endogenous HA receptor(s) (Boels et al., 2001). The experiment was repeated several times on different days yielding similar results. On average, the calculated energy-transfer efficiencies were in the range of 19.4±4.5%, indicating the close association of GPR37 and HA. Non-transfected cells were negative, and no transfer of signal was obtained if an antibody against the FLAG tag at the C-terminus of GPR37 was used (data not shown).

For visualisation of HA binding to GPR37, a fluorescent derivative of HA was produced. For this purpose, the fluorophore Cy3B was coupled to the -amino group of Lys7 of HA. The neuroblastoma cell line NH15-CA2, which reacts with HA (Ulrich et al., 1996) and endogenously expresses GPR37 (Fig. 3E), was used as positive control. Binding of Cy3B-labelled HA to NH15-CA2 cells was observed starting from a concentration of 50 nM, with optimal binding at 150 nM, achieved after incubation for 10 minutes at 37°C (Fig. 3F). Pre-incubation with unlabelled HA for 50 minutes prevented Cy3B-HA binding (Fig. 3G). Cy3B-labelled HA did not bind to HEK-T-REx–GPR37 cells without induction of GPR37 expression by doxycycline (Fig. 3H), but reacted after induction for 24 hours with doxycycline (Fig. 3I). Pre-incubation with unlabelled HA inhibited binding (Fig. 3J), demonstrating that the two ligands compete for the same receptor and that the receptor is either occupied or, more likely, internalised after interaction with HA.

HA induces an increase in Ca^{2+} mobilisation in cells expressing GPR37

To confirm the interaction of HA with GPR37, Ca^{2+} mobilisation was measured in CHO-K1 cells stably

transfected with apoaequorin as Ca^{2+} sensor and with the promiscuous G-protein subunit G 16 for signal enhancement. After reconstitution with the aequorin cofactor coelenterazine, agonist action was monitored as increase in bioluminescence (Stables et al., 1997). Since GPR37 was not sufficiently expressed in this cell line (CHO) by transient transfection, a stable cell line was established that, in addition to G 16 and apoaequorin, also expressed GPR37 (CHO-GPR37). Treatment of these cells with HA dose dependently led to an increase in Ca^{2+} mobilisation with an EC_{50} value of 3.3 nM (Fig. 4A). To our surprise, an endogenous response was also observed (Fig. 4A). Northern blots were negative, but immunocytochemistry (Fig. 4B) and western blots (Fig. 4C) probed with an antiserum against the very conserved intracellular C-tail confirmed presence of GPR37 in CHO cells. The hippocampal mouse cell line HT22, expressing GPR37 endogenously, was used as a positive control (Fig. 4C). The active monomeric form of GPR37 was predominantly present both in CHO-GPR37 and HT22 cells.

HA stimulates a current increase in frog oocytes expressing GPR37

In our hands, the frog oocyte system has proven to be very reliable and robust for studying the interaction of ligands with orphan GPCRs (Ignatov et al., 2003a; Ignatov et al., 2003b). Since HA signal transduction for mitotic stimulation is coupled to an inhibitory G protein (Kayser et al., 1998; Ulrich et al., 1996), frog oocytes were injected not only with complementary RNAs (cRNAs) coding for human GPR37, but also with cRNAs coding for the G-protein-coupled inwardly rectifying K^+ channel GIRK, which is activated by subunits of inhibitory G proteins (Kofuji et al., 1995). The concatemer between GIRK1 and GIRK2 (GIRK1/2) was chosen to enhance the current increase and improve the signal to noise ratio (Wischmeyer et al., 1997). Treatment with HA led to an additional increase in the basal inward current induced by changing the external bath medium to high K^+ in oocytes expressing GPR37 together with GIRK1/2 (Fig. 5A). A minute, negligible response was also obtained with medium alone (Fig. 5A). The effect of HA was concentration dependent, and a dose-response curve yielded an EC_{50} value of 5.6 nM (Fig. 5B). Since HA was diluted about twofold by addition to the oocyte bath medium, this EC_{50} value is in agreement with that obtained in the Ca^{2+}-mobilisation assay in CHO cells. Oocytes expressing GIRK1/2 without GPR37 were unresponsive to HA (Fig. 5B). Comparable dose-response curves were obtained from 30 oocytes.

HA signal transduction

One of the most prominent effects of HA is that it stimulates cells to enter mitosis (Hampe et al., 2000; Kayser et al., 1998; Ulrich et al., 1996). At the G2-mitosis transition, histone H3 is phosphorylated and is, therefore, an excellent marker for mitotic events. HEK-T-REx–GPR37 cells were incubated with and without doxycycline for 24 hours, before HA was added for 1.7 hours. Cells induced with doxycycline to express GPR37 showed an increase over uninduced cells in the percentage of mitotic cells, as visualised with the antibody against phosphorylated histone H3 (Fig. 6A). This suggested a direct role for GPR37 in mediating the action of HA as a mitogen. To monitor HA signalling mediated by GPR37, transiently transfected COS-7 cells and HEK-T-REx–GPR37 cells were subjected to electrophysiological analysis by patch clamping. Treatment of cells with HA led

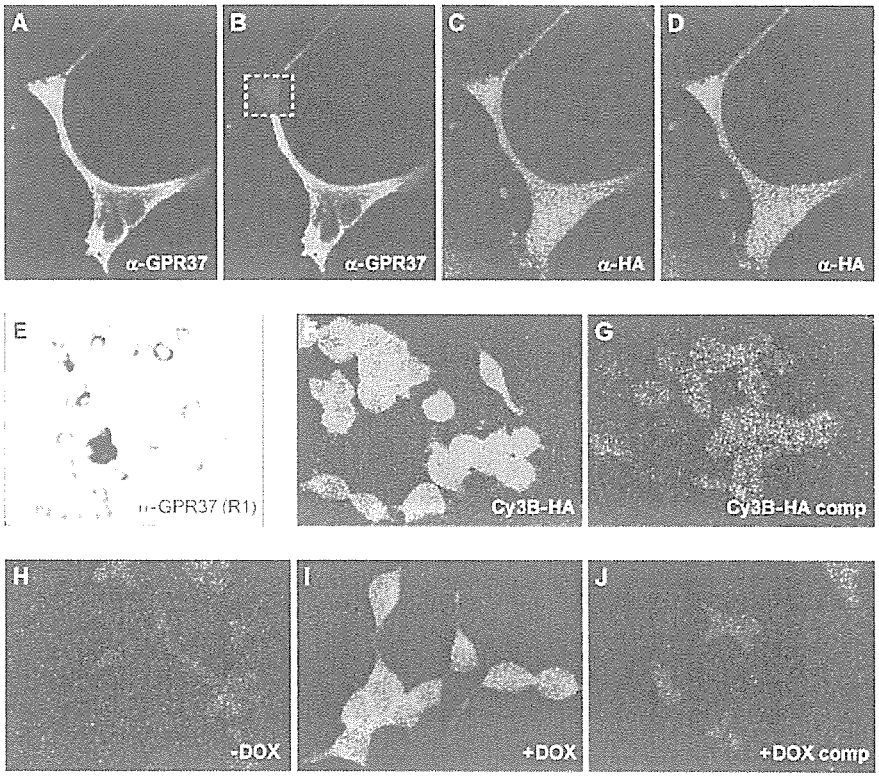

Fig. 3. HA colocalises with and binds to GPR37. (A-D) Interaction of HA and GPR37 analysed by FRET. Shown is a typical example of FRET between HA and an extracellular epitope of GPR37. COS-7 cells transiently transfected with GPR37 were treated with 2 nM HA for 20 minutes on ice to prevent internalisation, followed by incubation for 20 minute on ice with the antiserum against HA (-HA). After fixation with 4% formaldehyde in PBS, cells were immunostained with anti-GPR37 antibody (-GPR37). GPR37 immunoreactivity was visualised with Cy3 (A,B) and that of HA with Alexa Fluor 488 (C,D). (A) The Cy3 signal (GPR37) is shown after excitation at 568 nm. (B) A discrete area was photobleached using intense 568 nm laser. The Alexa Fluor 488 signal (HA) after excitation at 488 nm is shown before (C) and after (D) photobleaching. In this example, the Alexa Fluor 488 signal was increased by 18%. (E-G) The neuroblastoma cell line NH15-CA2 was used as a positive control to show specific Cy3B-HA binding to endogenous HA receptors. (E) NH15-CA2 cells endogenously express GPR37, as visualised with anti-GPR37(R1) antibody [-GPR37(R1)]. (F,G) Binding is optimal at 150 nM of Cy3B-HA after incubation for 10 minutes at 37°C (Cy3B-HA) and is inhibited by pretreatment for 50 minutes at 37°C with 100 nM unlabelled, monomerised HA (Cy3B-HA comp). (H-J) HEK-T-REx–GPR37 cells bound Cy3B-HA only after GPR37 induction with doxycycline (±DOX), and binding was competed with unlabelled HA (+DOX comp).

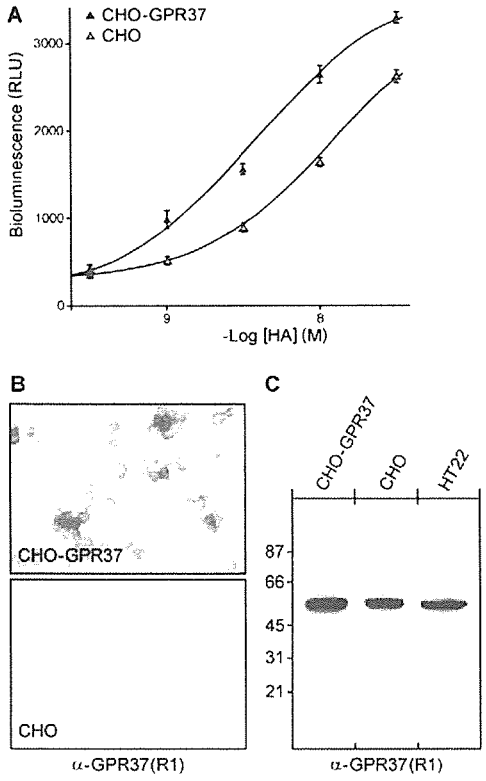

Fig. 4. HA stimulates Ca^{2+} mobilisation in CHO-K1 cells stably transfected with GPR37-FLAG, G 16 and apoaequorin. (A) The Ca^{2+}-bioluminescence response was measured at 469 nm and is expressed in relative light units (RLU), from which the medium response was subtracted. Values are given as means ± s.d. CHO-G 16-AEQ cells stably expressing GPR37-FLAG (CHO-GPR37) responded with an EC_{50} value of 3.3 nM; the endogenous response of CHO-G 16-AEQ cells (CHO) resulted in an EC_{50} value of 11 nM. Data show representative results of three independent experiments. (B) CHO-GPR37 (upper panel) and CHO cells (lower panel) reacted with anti-GPR37(R1) antibody [-GPR37(R1)], a polyclonal antiserum produced against the conserved intracellular C-tail. (C) Western blot analysis of membrane fractions confirmed an increased expression of GPR37 in transfected cells. The mouse hippocampal cell line HT22, expressing GPR37 endogenously, was used as a positive control.

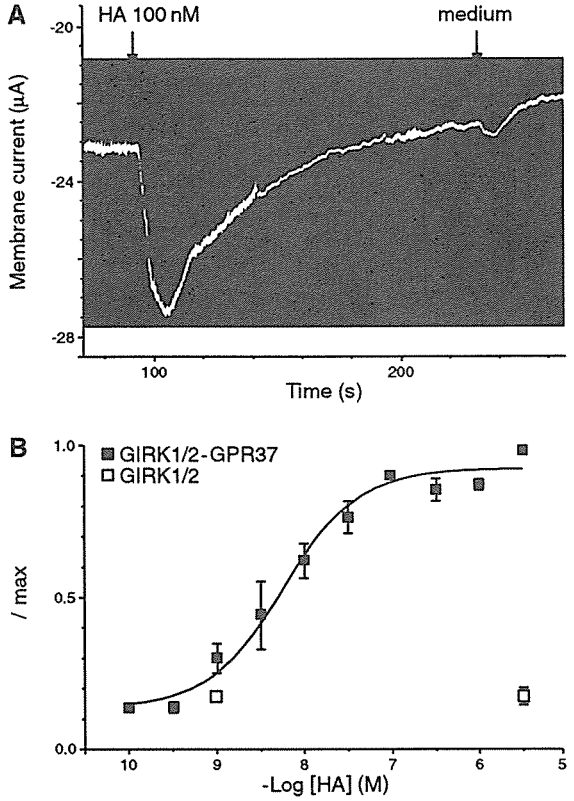

Fig. 5. HA is a high-affinity ligand for GPR37 expressed in frog oocytes. (A) Currents induced by 100 nM HA were recorded from *Xenopus* oocytes injected with cRNAs coding for GPR37 and for GIRK1/2. Stimulation with medium served as control. (B) The current increase was dependent on HA concentration. Dose-response curves for a HA-induced increase in GIRK1/2-mediated inward currents were normalised against maximal currents obtained for each oocyte. Current increases were averaged over four oocytes prepared and injected on the same day. The values represent means ± s.d. Data are representative of several independent experiments.

to an increase in membrane currents (Fig. 6B), which was blocked by La^{3+} and by SKF (Fig. 6B), both of which are known inhibitors of TRP-like Ca^{2+} channels. These Ca^{2+} channels, upon stimulation of receptors with ligands, translocate from an intracellular pool to the plasma membrane, for which activation of phosphoinositide 3-kinase (PI 3-kinase) and Ca^{2+}-dependent calmodulin (CaM) kinase is a prerequisite (Boels et al., 2001). The HA-induced increase in current was prevented by pre-incubating cells with pertussis toxin, wortmannin and KN93 (Fig. 6C), which demonstrates that an inhibitory G protein, PI 3-kinase and CaM-kinase II, respectively, are involved in the HA-GPR37 signalling cascade. A preliminary scheme of HA signalling is shown in Fig. 7.

Discussion

We present evidence that HA is a high-affinity ligand for GPR37. After heterologous expression in frog oocytes and in mammalian cells, EC_{50} values in the low nanomolar range were obtained. Electrophysiological analysis revealed that GPR37 activation by HA involved the same signalling cascade (Fig. 7) as found earlier for the endogenous HA receptor (Boels et al., 2001; Kayser et al., 1998; Ulrich et al., 1996). Interaction with HA resulted in GPR37 internalisation and stimulated entry into mitosis.

HA is bound to a carrier-like molecule both in hydra and in mammals, which improves the half-life and function of HA (Roberge et al., 1984; Schaller et al., 1996). The HA-binding protein HAB was isolated from hydra using HA-affinity chromatography, and later SorLA was discovered as an orthologue of HAB (Hampe et al., 2000). SorLA is a multi-ligand sorting receptor that, in addition to HA, binds glial-cell-derived neurotrophic factor (GDNF), PDGF and apolipoprotein E (ApoE) (Gliemann et al., 2004; Taira et al., 2001; Westergaard et al., 2004). HAB and SorLA are type I

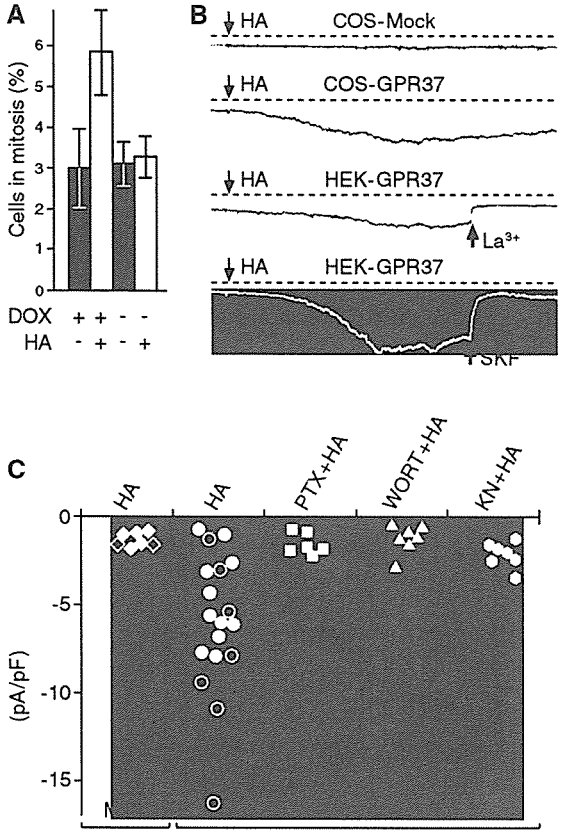

Fig. 6. GPR37 mediates HA signalling to stimulate mitosis. (A) HEK-T-REx–GPR37 cells were treated with and without doxycycline for 24 hours. Incubation with 2 nM HA for 1.7 hours led to an increase of cells in mitosis after induction of GPR37 expression. Immunostaining of cells with anti-phospho-histone H3 (1:1000) was used to determine cells in mitosis. 6 350 cells were counted, and the percentage of stained mitotic cells is given as means ± s.d. (B) Membrane currents were measured in the perforated patch configuration at a holding potential of –80 mV. Treatment with 1 nM HA induced an increase in membrane currents in COS-7 cells transiently expressing GPR37 (COS-GPR37), but not in mock-injected cells (COS-Mock). Membrane currents activated by HA in HEK-T-REx–GPR37 cells were blocked by application of 1 mM La^{3+} or 10 M SKF. (C) Membrane-current densities were recorded from mock- and GPR37-transfected COS-7 cells. HA signal transduction was inhibited by pretreating cells for 2-3 hours with 200 ng ml^{-1} pertussis toxin (PTX), for 30-60 minutes with 100 nM wortmannin (WORT), or 30 M KN93 (KN). Each symbol represents one cell measured in the whole-cell (filled symbols) or the perforated patch (open symbols) configuration

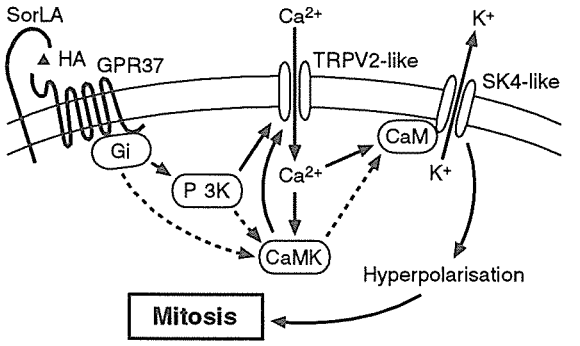

Fig. 7. Scheme of the signalling pathway from HA through GPR37 to stimulate mitosis. After binding of HA to GPR37 with or without help of the coreceptor SorLA, a pertussis-toxin-sensitive inhibitory G protein (Gi) is activated, which interacts through the phosphoinositide 3-kinase (PI3K) and the calcium-calmodulin dependent kinase II (CaMK) with a Ca^{2+} channel of the transient receptor potential family (TRPV2-like). The resulting Ca^{2+} influx activates a Ca^{2+}-dependent K^+ channel of the small and intermediate conductance family (SK4-like), leading to hyperpolarisation, which is a prerequisite for cells to enter mitosis. Dashed lines indicate hypothetical pathways.

transmembrane receptors with a large extracellular domain that can be shed by metalloprotease cleavage (Hampe et al., 2000). This represents an ideal mechanism to regulate the range of action of a morphogen like HA. GPR37 contains a relatively large extracellular domain, which is unusual for a peptide receptor. The notion that SorLA interacts with this domain of GPR37 as co-receptor to enhance HA binding (Hampe et al., 2000) is plausible and outlined in Fig. 7.

GPCRs play key physiological roles, and their dysfunction is implicated in several diseases. This might be reflected by the fact that about half of the current drugs, and certainly more in the future, are targeted to these receptors. GPR37 is of special interest for pharmacology, since it was shown to contribute to Parkinson's disease. GPR37 was characterised as a substrate for the E3 ubiquitin ligase parkin (Imai et al., 2001). Ubiquitylation marks proteins for degradation. Parkin mutations have been shown to be causative for neurodegeneration in Parkinson's disease, where dopaminergic neurons of the substantia nigra are especially affected (Imai et al., 2001; Yang et al., 2003). We found that overexpression of GPR37 resulted in complexes of molecular masses 250 kDa. Aggregated GPR37 did not translocate to the cell surface, as shown by cell-surface biotinylation experiments, and most probably led to preferential cell death of transfected cells. We could express GPR37 successfully in frog oocytes and in mammalian cells after stable integration into the chromosome. Since frog oocytes are cultured at room temperature, more time for proper folding may have been advantageous for GPR37 expression. Similarly, lower levels of GPR37 transcripts by stable expression may have caused less stress for the cells. The fact that insoluble GPR37 was enriched in brains of patients with juvenile Parkinson's disease (Imai et al., 2001) and its presence in Lewy bodies (Murakami et al., 2004) supports the notion that GPR37 misfolding contributes to neuronal cell death (Imai et al., 2003). This might be confirmed by the recent finding that GPR37-knockout mice showed altered dopaminergic signalling and were resistant to the neurotoxin 1-methyl-4-phenyl-1,2,3,6-tetrahydropyridine (MPTP), which preferentially kills dopaminergic neurons (Marazziti et al., 2004). As SorLA was found to be downregulated in the brains of patients with Alzheimer's disease (Scherzer et al., 2004), it is intriguing to speculate that a connection exists between SorLA, GPR37 and HA to improve neuronal cell survival.